UPPSALA
UNIVERSITET

Digital Comprehensive Summaries of Uppsala Dissertations from the Faculty of Science and Technology 271

Heavy-Core Staffanes

A Computational Study of Their Fundamental Properties of Interest for Molecular Electronics

NICLAS SANDSTRÖM

ACTA
UNIVERSITATIS
UPSALIENSIS
UPPSALA
2007

ISSN 1651-6214
ISBN 978-91-554-6796-8
urn:nbn:se:uu:diva-7492

Dissertation presented at Uppsala University to be publicly examined in B22, BMC, Husargatan 3, Uppsala, Wednesday, March 7, 2007 at 13:15 for the degree of Doctor of Philosophy. The examination will be conducted in Swedish.

Abstract

Sandström, N. 2007. Heavy-Core Staffanes. A Computational Study of Their Fundamental Properties of Interest for Molecular Electronics. Acta Universitatis Upsaliensis. *Digital Comprehensive Summaries of Uppsala Dissertations from the Faculty of Science and Technology* 271. 80 pp. Uppsala. ISBN 978-91-554-6796-8.

The basic building blocks in molecular electronics often correspond to conjugated molecules. A compound class consisting of rigid rod-like staffane molecules with the heavier Group 14 elements Si, Ge, Sn and Pb at their bridgehead positions has now been investigated. Herein these oligomers are called heavy-core or Si-, Ge-, Sn- or Pb-core staffanes. These compounds benefit from interaction through their bicyclo[1.1.1]pentane monomer units. Quantum chemical calculations were performed to probe their geometries, stabilities and electronic properties associated with conjugation.

The stabilities of the bicyclo[*n.n.n*]alkane and [*n.n.n*]propellanes ($1 \leq n \leq 3$) with C, Si, Ge and Sn at the bridgehead positions were studied by calculation of homodesmotic ring strain energies. The bicyclic compounds with $n = 1$ and Si, Ge or Sn at bridgehead positions have lower strain than the all-carbon compound.

A gradually higher polarizability exaltation is found as the bridgehead element is changed from C to Si, Ge, Sn or Pb. The ratio between longitudinal and average polarizability also increases gradually as Group 14 is descended, consistent with enhanced conjugation in the heavier oligomers.

The localization of polarons in C-, Si- and Sn-core staffane radical cations was calculated along with internal reorganization energies. The polaron is less localized in Si- and Sn-core than in C-core staffane radical cation. The reorganization energies are also lower for the heavier staffanes, facilitating hole mobility when compared to the C-core staffanes.

The effect of the bicyclic structure on the low valence excitations in the UV-spectra of compounds with two connected disilyl segments was also investigated. MS-CASPT2 calculations of 1,4-disilyl- and 1,4-bis(trimethylsilyl)-1,4-disilabicyclo[2.2.1]heptanes and 1,4-disilyl- and 1,4-bis(trimethylsilyl)-1,4-disilabicyclo[2.1.1]hexanes revealed that although the bicyclic cage separates the two disilyl chromophores, there is a strong red-shift of the lowest valence excitations when compared to an isolated disilane.

Keywords: conjugation, polarizability, Group 14 elements, cage compounds, electronic excitations, quantum chemistry, molecular electronics

Niclas Sandström, Department of Biochemistry and Organic Chemistry, BMC, Box 576, Uppsala University, SE-75123 Uppsala, Sweden

ISSN 1651-6214
ISBN 978-91-554-6796-8
urn:nbn:se:uu:diva-7492 (http://urn.kb.se/resolve?urn=urn:nbn:se:uu:diva-7492)

List of papers

I **Heavy Group 14 1,(*n*+2)-Dimetallabicyclo[*n.n.n*]alkanes and 1,(*n*+2)-Dimetalla[*n.n.n*]propellanes: Are They All Realistic Synthetic Targets?** N. Sandström, H. Ottosson*. *Chem. Eur. J.* 2005, *11*, 5067-5079.

II **In Search of 1,3-Disila/germa/stannabicyclo[1.1.1]pentanes with Short Bridgehead-Bridgehead Distances and Low Ring Strain Energies.** J. Tibbelin, N. Sandström, H. Ottosson*. *Silicon Chem.* 2005, *3*, 165-173.

III **Heavy-Core Staffanes: Molecular Wires with an Unusual -Conjugation.** N. Sandström, J. R. Smith, H. Ottosson*. Submitted manuscript.

IV **Will Heavy-Core Staffanes Function as Hole transporting Molecular Wires? A Computational Investigation.** A. M. El-Nahas, N. Sandström, H. Ottosson*. Manuscript.

V **Lowest Valence Electronic Excitations of 1,4-Disilyl Substituted 1,4-Disilabicycloalkanes: A MS-CASPT2 Study on the Influence of Cage Size.** N. Sandström, C. M. Piqueras, H. Ottosson*, and R. Crespo*. Submitted manuscript

Reprints were made with permissions from the publishers.

Contribution Report

The author wishes to clarify his contribution to the included papers I-V:

I Partly formulated the research problem. The two authors equally shared the computational work, interpretations of results and writing of the manuscript.

II Significant part of the computational work and significant contribution to evaluation of the results.

III Partly formulated the research problem, significant part of computations and evaluation of results, and partly wrote the manuscript.

IV Partly performed computational work and evaluation of the results.

V Partly formulated the research problem. Performed all the calculations, significant part of evaluation, and significant part of the writing of the manuscript.

Contents

Abbreviations

6-31G(d)	Pople basis set
6-31G(+sd+sp)	Pople basis set with Spackman's polarization- and diffuse functions (basis set)
a.u.	Atomic units
α_{avg}	Average polarizability
ANO	Atomic Natural Orbitals (basis set)
AO	Atomic Orbitals (approximation)
α_{zz}	zz-Component of second rank polarizability tensor, longitudinal polarizability
α_{zz}^{n}	Longitudinal polarizability for the oligomer consisting of *n* monomer units
γ_{zz}	Average longitudinal polarizability
B3LYP	Becke-3 + LYP hybrid functional (method)
BD	Brueckner Doubles (method)
BO	Born-Oppenheimer (approximation)
β_{zzz}	zzz-Component of third rank hyperpolarizability tensor
CASPT2	Complete Active Space second order Perturbation Theory (method)
CASSCF	Complete Active Space SCF (method)
CC	Coupled Cluster (theory)
cc-pV*n*Z	Correlation Consistent Polarized Valence *n*-Zeta, *n* = level of contraction (basis set)
CCSD	Coupled Cluster Singles Doubles (method)
CCSD(T)	Coupled Cluster Singles Doubles and perturbative Triples (method)
CGTO	Contracted Gaussian Type Orbital Function
CI	Configuration Interaction (theory)
CISD	Configuration Interaction Singles Doubles (method)
CPHF/CPKS	Coupled Perturbed Hartree-Fock/Kohn-Sham (method)
$\Delta\alpha_{zz}$	Longitudinal polarizability difference
ΔE	Energy difference
DFT	Density Functional Theory
ECP	Effective Core Potential (approximation)
EPR	Electron Paramagnetic Resonance (technique)
F	Electric field
f	Oscillator Strength

FCI	Full CI (method)
FF	Finite Field (method)
GGA	Generalized Gradient Approximation
$_{GS}$	Irreducible representation of the ground state
$_{p}$	Irreducible representation of the dipole operator
$_{Sym}$	Totally symmetric irreducible representation
GTO	Gaussian type Orbital Function
$_{XS}$	Irreducible representation of the excited state
HDE	Homodesmotic ring strain Energy
HF	Hartree-Fock (theory)
HK	Hohenberg-Kohn (*anzats*)
HMO	Hückel Molecular Orbitals (theory)
HOMO	Highest Occupied Molecular Orbital
IP	Ionization Potential
k_{CT}	Charge transfer rate
KS	Kohn-Sham
!	Power dependence
LANL2DZ	Los Alamos National Laboratory 2nd Double-Zeta (ECP)
LANL2DZdp	Los Alamos National Laboratory 2nd Double-Zeta plus Diffuse and Polarization (ECP+basis set)
LANL2DZp	Los Alamos National Laboratory Polarization (ECP+basis set)
LCAO-MO	Linear Combinations of Atomic Orbitals to Molecular Orbitals (approximation)
LDA	Local Density Approximation
$!_{i}$	Internal reorganization energy
$!_{s}$	Solvent reorganization energy
LSDA	Local Spin Density Approximation
LUMO	Lowest Unoccupied Molecular Orbital
LYP	Lee, Yang and Parr (method)
MCSCF	Multi-Configurational Self-Consistent Field (method)
Me	Methyl
MMe_2	Dimethylmetalene
MO	Molecular Orbital
MP4(SDTQ)	Møller-Plesset Perturbation Theory including single-, double-, triple and quadruple excitations (method)
MP*n*	Møller-Plesset Perturbation Theory, *n*=1, 2, 3, 4, … (method)
MS-CASPT2	Multi-State Complete Active Space second order Perturbation Theory (method)
NBO	Natural Bond Orbital (method)
n-doping	Negative doping (reduction)
NDR	Negative Differential Resistance
nm	Nanometer (length unit)
NO	Natural Orbitals
NPA	Natural Population Analysis (method)

PBE0	Functional (DFT)
p-doping	Positive doping (oxidation)
PGTO	Primary Gaussian type Orbital Function
PMCAS	Perturbed Modified Complete Active Space
PMe	Methyl phosphinyl
POL	Sadlej's basis set
Q	Quadrupole moment
RHF	Restricted Hartree-Fock (method)
ROVGF	Restricted Outer Valence Green's Function (method)
SAM	Self-Assembled Monolayer
SCF	Self-Consistent Field
SD	Slater Determinant
SDB	Stuttgart–Dresden–Bonn (ECP)
SPM	Scanning Probe Microscope (technique)
STM	Scanning Tunneling Microscope (technique)
STO	Slater Type Orbital
T	Temperature
TDM	Transition Dipole Moment
TMS	Trimethylsilyl
UHF	Unrestricted Hartree-Fock (method)
UV/Vis	Ultraviolet/Visual (wavelength range)
V	Electronic coupling term
ZPE	Zero Point Energy Corrections
Å	Length unit

1. Introduction

In 1998 the Nobel Prize in chemistry was awarded to John Pople and Walter Kohn for their groundbreaking work in quantum chemistry,[1] which over the preceding decades had enabled both quantitative and qualitative solutions to problems faced in other fields of chemistry. Besides advances in theory and computational algorithms the development of computer technology has been crucial for the advances of computational quantum chemistry. However, the miniaturization of the basic computer component, the microchip, will eventually reach the physical limit of the current silicon based technology. At this stage, could quantum chemical calculations in return provide a tool for the further development of even smaller building blocks for making electronic circuitry for tomorrow's computers?

Gordon Moore made a prediction for the future development of integrated circuits in 1965;[2] ten years later this became known as *Moore's law*. It has since then been modified, as well as interpreted and misinterpreted in different ways. The most common version states that the number of integrated components on a silicon chip, which is put on the market, doubles every 18th month. Further miniaturizations of the components on a silicon wafer will either not be physically possible, or the cost will be too high. At that stage the search for new materials and manufacturing approaches must have found new approaches if the electronics industry should keep its present pace. Thus, there is a demand for new technology, and molecular electronics is one possible candidate for such technology.

1.1. Molecular Electronics – A Short Historical Background

The concept of miniaturizing devices is not new. In 1959 Richard Feynman presented a talk entitled "*There is Plenty of Room at the Bottom*" where he proposed devices made out of only ten to a hundred atoms.[3] The idea of making small computers was given as one of the examples:

> "Why can't we make them (computers) very small, make them of little wires, little elements---and by little, I mean *little*. For instance, the wires should be 10 or 100 atoms in diameter, and the circuits should be a few thousand ångströms across."

Fifteen years later another milestone in molecular electronics was put forward,[4] when Aviram and Ratner proposed an organic molecule, *Figure 1*, for which they calculated rectifying properties, i.e. a molecular diode.

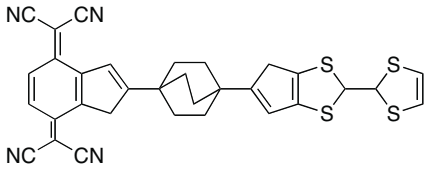

Figure 1. Proposed molecular rectifier where the electron-donor part is to the right (tetrathiafulvalene) and electron-acceptor part the left (tetracyanoquinodimethane), separated by bicyclo[2.2.2]octane in the middle.

The idea was to have a -electron donor - acceptor system where the donor and acceptor are linked by a ! -bonded bridge. If both ends of the molecule were connected to metal contacts and an electric field was applied, the probability of tunneling electrons through the ! -bonded bridge should be much higher going from acceptor to donor than vice versa, *Figure 2*.

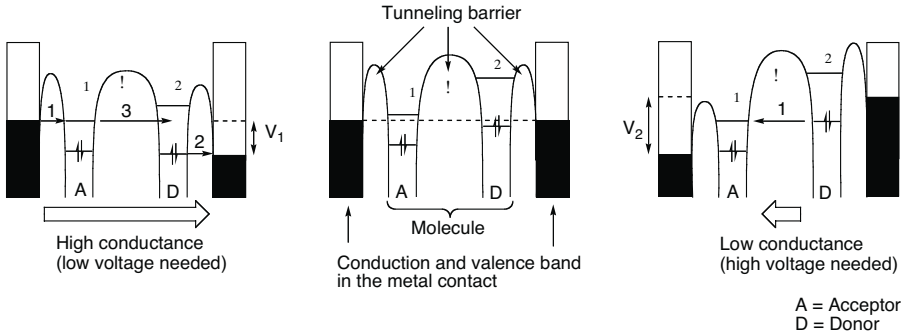

Figure 2. Rectifying mechanism proposed by Aviram and Ratner for a single molecular donor-acceptor system.

The experimental progress took off in the 80's with the improvements of the *scanning tunneling/probe microscope* (STM/SPM) technique, which made it possible to measure the conductance of a small bundle of molecules in a self-assembled monolayer (SAM), *Figure 3*.

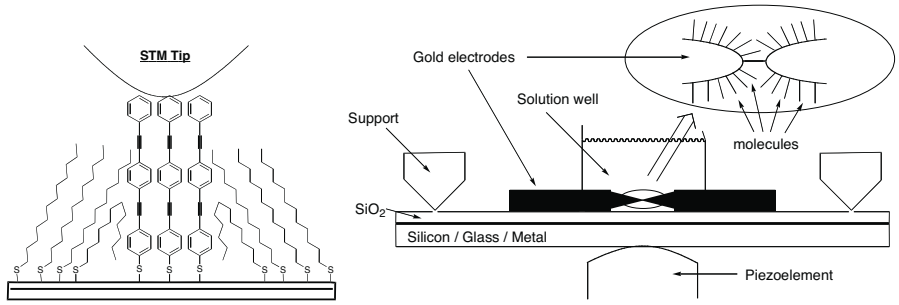

Figure 3. Schematic pictures of the general set-up for STM (left) and break junction (right)

Further refinement of conduction measurements of single molecules came in 1997 when Reed *et al.* introduced the break-junction technique,[5] where a molecule is stretched between two gold electrodes, *Figure 3*.

The molecules that have been investigated and shown conduction, rectifying properties or negative differential resistance (NDR) are mainly different types of -bonded systems, *Figure 4*. Molecules utilizing geometrical changes to cause switching of the rectifying properties have also been proposed.[6]

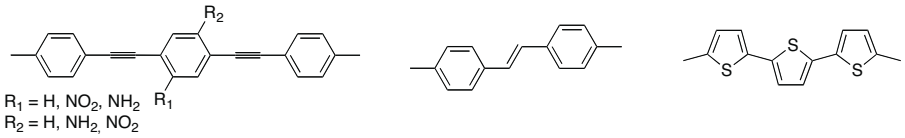

Figure 4. Examples of compounds used in conductivity measurements. From left: oligophenylene-ethylene (OPE), oligophenylene-vinylene (OPV), and oligothiophene.

The accumulated development in techniques and experimental results lead Science Magazine in 2001 to announce molecular electronics research as the "Breakthrough of the year".[7] The most optimistic voices envisioned molecular electronic devices in the marketplace within a four-year period. However, it was soon revealed that some data were published without proper reference experiments and there were even cases of fraud.[8] So in 2003 Science Magazine questioned if molecular electronics had hit an "Early midlife crisis?".[9] Since then the view of the possibilities and problems in the molecular electronics research field have become more balanced. However, the research field is still young and there are a number of important questions that needs to be answered, such as how to arrange molecules in the positions where one wants them, i.e. the field of molecular recognition and self-organization. Connectivity is also an issue, currently the smallest objects that can be made, by top-down approaches, using e-beam lithography are around 30 nm.[10] This

is a relatively large gap when compared to e.g. the diameter of a carbon nanotube which is around 1-2 nm.[11] The question about the viability to make single molecular devices has also been raised, since the thermal fluctuation in any chemical system at room temperature makes a device likely to be unreliable. If there is to be a mass-market technology based on molecular electronics, at any time in the future, it ultimately depends on manufacturing costs. It has to be cheaper than the existing technology, since economy is a major driving force.

1.2. Towards Novel Building Blocks for Molecular Electronics

The aim of the studies in this thesis has been to investigate the properties of novel, potentially conjugated, molecules so as to expand the number of building blocks available to molecular electronics. Of special interest is the basic wire, a molecule facilitating the movement of a charge from one end to the other. As mentioned above, the molecules that have shown the most promising conducting properties are conjugated.[12]

1.2.1. Conjugation

Conjugation is a concept often used to explain various observations in chemistry. However, from a quantum mechanical point of view conjugation is not a property for which there is an operator that can act on a wavefunction, giving an absolute value. Instead, conjugation is described through models which provide associated measurable properties.

Hückel model

Using the Hückel molecular orbitals (HMO) model to describe conjugated -systems gives rise to interesting observations. In a -system the -bonds can interact in two different ways, in-phase or out-of-phase, *Figure 5*. Bonding orbitals in-phase give rise to an energetically favorable interaction, whereas the out-of-phase combination do the contrary. The opposite applies to antibonding orbitals.

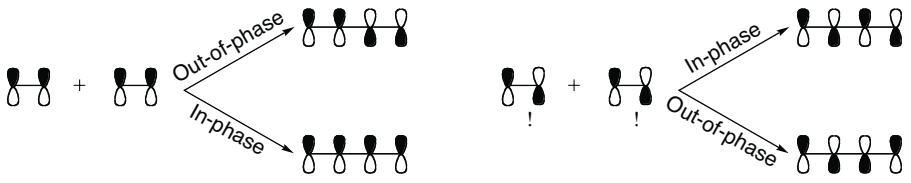

Figure 5. Two different ways to combine bonding ( ) and antibonding (*) -orbitals.

Consider now a linear polyethylene molecule, as an example, and regard how the molecular orbital (MO) energy levels evolve as the number of repeat units grow, *Figure 6*. With this model the polymer at infinite length obtains a band structure and can become metal-like since the highest occupied MO (HOMO) match the energy of the lowest unoccupied MO (LUMO).

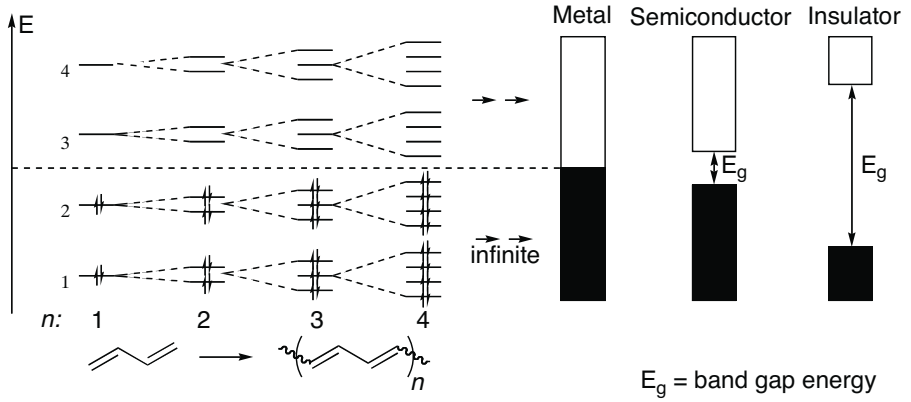

Figure 6. Splitting of MO-energy levels ( ) due to favorable and unfavorable orbital interactions with the growth of the polymer chain, which in HMO-theory leads to metal-like band structure, whereas in reality the semiconductor and insulator band structures are predominant.

However, the realization of a conjugated molecular wire with a truly metallic character is very hard to accomplish; organic polymers are insulating or at best semi-conductors, with a few exceptions.[13] This means that there is a energy gap between the HOMO (valence band) and the LUMO (conduction band), *Figure 6*. A semiconductor is generally considered to have a band gap of less than 2 eV at room temperature, and materials with a larger band gap are regarded as insulators.[14]

A fully delocalized electron distribution, as in a metal-like polymer, would also imply that all C-C bonds are of equal length. The source for the distortion from the geometry with equal bond length to one with alternating bond-lengths as in polyethylene is the Jahn-Teller distortion, in condensed matter physics known as Peierls distortion. This stems from electron-electron repulsion, which is neglected in the HMO model, and which localizes electrons in the C=C double bonds with an energy gain as the driving force.

Alternative models

Beside the Hückel MO model for rationalization of conjugation, other methods can also be applied to determine if the compound is conjugated or not. *Natural bond orbital* (NBO) analysis for example, has been used to describe

different conjugation pathways in variously cross-conjugated -bonded molecules, that only differ in their conformation.[15]

Beside computational models there are measurable properties connected to conjugation, such as UV/Vis absorption (optical band gap measurements), ionization potentials, polarizabilities, and the ability to delocalize charge etc. that change with the degree of conjugation.

#-Conjugation

Most conducting molecules consist of ordinary -conjugated systems like aromatic rings, including thiophenes and pyrroles, which often are connected via ethylene or ethenyl bridges. Beside the -conjugated systems there are molecules with a different conjugation topology, so-called #-type conjugation. Examples of such species are oligosilanes and oligostannanes, i.e. heavy alkanes. The *ladder* model can give a rational explanation to #-conjugation by considering the different #-orbital interactions, *Figure 7*.[16] Using the same reasoning as for polyethylene, the band gap decreases with the length of the polymer. Experimentally, the wavelength of the UV-absorption maxima for peralkylated polysilanes decreases as the polymer length is increased up to a saturation value at 300 – 325 nm, depending on substituents on Si.[17] However, the conjugation and thus the absorption maxima, has a strong conformational dependence. To show maximum conjugation the oligomer must be in its all-anti conformer, *Figure 7*.

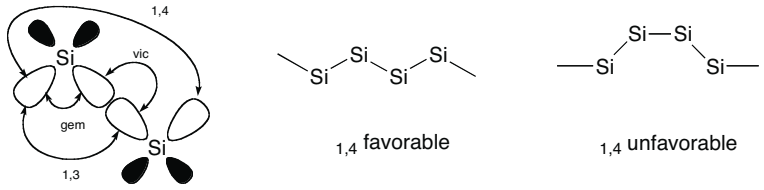

Figure 7. Schematic representations of orbital interactions (!) in polysilane described in the ladder model (left). Anti (middle) and gauche (right) conformers of tetrasilane. The former shows better conjugation properties. Substituents on Si omitted for clarity.

Any twist in the chain will lead to shorter effective conjugation length and the excitation becomes confined to a shorter segment of the chain, i.e. Anderson localization.[18] This has been proven both experimentally and computationally.[17,19]

The conjugation properties of the oligosilanes/stannanes are promising, but the conformational flexibility makes them less suitable as single molecular wires.

1.2.2. Staffanes

Molecules that have very little conformational freedom are staffanes, *Figure 8*. The general structure of staffanes is that of an oligomer composed of bicyclo[1.1.1]pentane repeat units, and they have been described as molecular rods.[20]

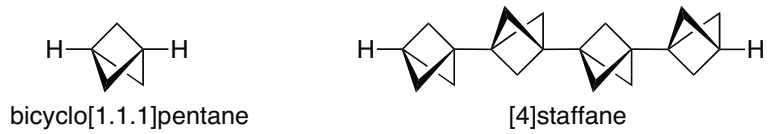

Figure 8. Molecular structure of bicyclo[1.1.1]pentane and [4]staffane.

Apart from being well-defined in length and directionality, bicyclo[1.1.1]pentane and staffanes also exhibit other interesting features. It has been shown from both experimental and theoretical investigations that there is through-space coupling in bicyclo[1.1.1]pentane and short staffanes. In solvolysis experiments the rate of dissociation of Br at the 3-position was influenced by the substituent in the 1-position, and this has been attributed to the through-space interaction.[21] Electron paramagnetic resonance (EPR) experiments on [1] – [3]staffayl radicals show that the bridgehead carbon atoms couple and that the spin densities couple through the cage structure, *Figure 9*.[22]

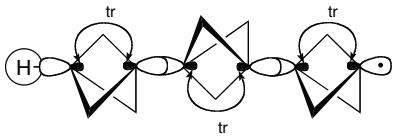

Figure 9. Schematic picture of through-space coupling ($_{tr}$) in [3]staffyl radical.

For the [1]staffyl radical the hyperfine splitting constant, due to !-coupling with hydrogen, is as high as 69.6 G. The same coupling over two cages decreases to 3.0 G and over three cages down to 0.1 G. A modified NBO-analysis showed that between 2/3 and 3/4 of the coupling is through-space and the rest through the C-C bonds of the methylene tethers.

The conformational rigidity of the staffanes together with the #-conjugation in heavy alkanes would be a desirable combination.

1.2.3. Heavy-Core Staffanes

Exchanging the bridgehead C-atoms in the staffanes to heavier Group 14 elements, creates a novel class of compounds that we call *heavy-core staf-*

fanes, *Figure 10*. The heavy-core staffane is still rod-like and well defined in space, but the heavier Group 14 bridgehead would introduce interesting changes of properties compared to all-carbon staffanes.

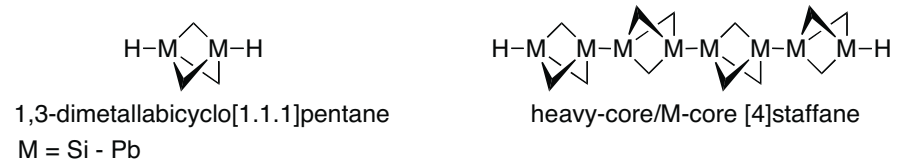

Figure 10. Molecular structure of 1,3-dimetallabicyclo[1.1.1]pentane and heavy-core M-core [4]staffane.

The through-space distance between the two bridgehead Group 14 atoms within one repeat unit is kept short by the methylene tethers and it is comparable to the M-M single bond length. Upon moving down Group 14 the atoms become larger and have more polarizable electron distributions. Combining these two effects could give rise to an increase of the through-space interaction between the bond orbital back lobes of the M-M bond orbitals. If these effects were sufficiently strong the heavy-core staffanes would exhibit conjugation-type properties, well in the range of polysilanes.

The 1,3-dimetallabicyclo[1.1.1]pentanes have structural similarities to the all-carbon analogue, bicyclo[1.1.1]pentane, which is a ring-strained molecule with known properties. By comparing the different M substituted 1,3-dimetallabicyclo[1.1.1]pentanes to bicyclo[1.1.1]pentane the relative ring strain, together with some aspects of reactivity can be estimated and rationalized for the Group 14 elements. This would elude whether to pursue them synthetically, or not. Electronic properties can also be computed for the heavy-core staffanes and compared to oligomer compounds with known good conjugation to get an estimate of their potential as molecular conductors.

2. Quantum Chemical Methods

Almost eighty years have passed since Heitler and London[23] first used quantum mechanics to rationalize the bonding in the hydrogen molecule. Since then its use has grown and successful applications can be found in many areas of chemistry. The developments of efficient algorithms and computer code, in combination with the fast development of computer performance, are contributing factors to the increasing popularity of quantum chemistry. One of the more appealing features with treating a chemical problem quantum chemically is the possibility of prediction. Molecular stability, spectroscopic properties and chemical reactivity are examples of features that can be modeled with quantum chemical methods. This said, there are still many areas where quantum chemistry is unable to quantitatively or even qualitatively predict or explain chemical properties since chemical systems may be very complex in their nature, beyond the approximations developed up to this date.

The following chapter will briefly describe the quantum chemical methods, with their approximations and applications, which are used in the work described in this thesis. For more elaborate descriptions in this field, the reader is directed to the references "*Introduction to Computational Chemistry*" (by F. Jensen, Wiley, 1999), "*Molecular Electronic-Structure Theory*" (by T. Helgaker, P. Jorgensen, J. Olsen, Wiley, 2000) and "*A Chemist's Guide to Density Functional Theory 2nd Ed.*" (by W. Koch, M. C. Holthausen, Wiley, 2002).

2.1. Molecular Orbital Theory

To quantum mechanically describe a molecular system, the nuclei and the electron distribution, the starting point is the Scrödinger equation which in a general form can be written as

$$\mathbf{H} = E \tag{2.1}$$

where **H** is the Hamiltonian operator acting on , the wavefunction describing the system, giving *E*, the corresponding energy eigenvalue to . In this general form it is dependent on nuclear and electron coordinates and time. The time-dependence can be expressed as a phase factor and (2.1) can be

written as the time-independent Schrödinger equation which only depends on the positions of nuclei and electrons.

The Hamiltonian operator consists of several parts that take care of both the potential and kinetic energies of the nuclei and electrons. Usually two approximations to this nuclei-electron system are performed to simplify the solution of the Schrödinger equation. First, one decouples all interactions between different electronic states, the so-called *adiabatic* approximation. The second approximation is the Born-Oppenheimer (BO) approximation, in which it is assumed, because of the large difference in weight between the nuclei and an electron, that the correlated movement between these two can be neglected. In a practical sense this implies that for any change in nuclear position the electronic relaxation is instantaneous.

The Hamiltonian operator for the molecular system can then be written as

$$\mathbf{H} = \mathbf{T}_e + \mathbf{V}_{ne} + \mathbf{V}_{ee} + \mathbf{V}_{nn} \qquad (2.2)$$

where $\mathbf{T}_e$ is the operator for the kinetic energy, $\mathbf{V}_{ne}$ the potential energy between nuclei and electrons, $\mathbf{V}_{ee}$ the potential energy between the electrons, and $\mathbf{V}_{nn}$ the repulsion between nuclei. As it turns out (2.1) cannot be solved exactly for any system consisting of more than one electron, so a numeric solution has to be found for any larger system. Fock and Slater, building on the work of Hartree, put such a solution forward.

2.1.1. Hartree-Fock Approximation

In the Hartree-Fock (HF) procedure the basic assumption is that every electron moves in an average electric field of all other electrons, i.e. an independent particle model.

To fully describe an electron wavefunction one not only has to know its kinetic and potential energy, its spin state must also be treated. The Hamiltonian operator (2.2) has no information about the spin, so this information is included implicitly in the wavefunction . The $\mathbf{x}_i$ includes all the parameters of electrons, spatial coordinates and spin. A molecular orbital (MO) is a spatial orbital combined with a spin function ! or #, resulting in a spin orbital % As electrons are fermions with spin ±1/2, any wavefunction has to be antisymmetric with respect to an interchange of two electrons, i.e. the wavefunction has to change sign if two electrons change place. A way to construct such a wavefunction is through a Slater determinant (SD) (2.3).

$$(x_1, x_2, ..., x_N) = \frac{1}{\sqrt{N!}} \begin{vmatrix} !_1(x_1) & !_2(x_1) & \cdots & !_N(x_1) \\ !_1(x_2) & !_2(x_2) & \cdots & !_N(x_1) \\ \vdots & \vdots & & \vdots \\ !_1(x_N) & !_2(x_N) & \cdots & !_N(x_N) \end{vmatrix} \quad (2.3).$$

A simpler way to write a SD is using the Dirac notation $\#_N(\mathbf{x}_N)!$. The Hamiltonian can be rewritten as an effective one-electron operator, a *Fock* operator

$$\mathbf{F}_i = \mathbf{h}_i + \sum_j^N (\mathbf{J}_{ij} ! \mathbf{K}_{ij}) \quad (2.4)$$

where $\mathbf{h}_i$ is the one-electron operator that takes care of the kinetic energy of electron i as well as its interaction with the nuclei, the $\mathbf{J}_{ij}$ operator describes the repulsive Coulomb interaction between the electrons i and j, and $\mathbf{K}_{ij}$ is the exchange operator. The occurrence of $\mathbf{K}_{ij}$ is a consequence of the antisymmetry principle in the SD and is only in effect between electrons of the same spin.

To be able to calculate the optimal HF wavefunction, a set of spin orbitals needs to be determined. Using the variational principle, any set of will lead to higher or, at the best, equal energy as the exact energy of the system. So the problem becomes to minimize the energy of the wavefunction and at the same time keep the spin orbitals orthonormal. This results in the HF equations, where Lagrange multipliers are used in the minimization to keep the orthonormality. The HF-equation can be rewritten to the canonical HF equations. To more easily solve this equation, in the case of closed-shell molecules, the spin can be projected out and the spin orbitals (**x**) can be replaced with spatial orbitals (**r**). This results in the restricted HF (RHF) equation

$$\mathbf{f}_i \; _i(\mathbf{r}) = !_i \; _i(\mathbf{r}) \quad (2.5).$$

Here the Lagrange multipliers $!_i$ can be interpreted as the MO energies, and since the *Fock* operator is dependent on the orbitals, (2.5) must be solved iteratively. Using the SD in (2.1) the electronic energy of the Hamiltonian (2.2) can be rewritten as (remembering that here J_{ij} and K_{ij} are two electron integrals)

$$E = \sum_i^N \#_i ! \frac{1}{2} \sum_{ij}^N (J_{ij} ! K_{ij}) \quad (2.6).$$

If one wishes to calculate an open-shell system, two sets of *Fock* equations appear after integrating out the spin functions, one for and one for *!* . This procedure is referred to as unrestricted HF (UHF). These two *Fock* matrices are dependent on each other and cannot be solved independently, which complicates the calculation. However, as UHF has a higher degree of variational freedom, the energy from a UHF calculation will be lower or equal to the RHF energy.

To solve (2.5) one treats the equation as a matrix eigenvalue problem given that one first makes the LCAO-MO (Linear Combination of Atomic Orbitals to Molecular Orbitals) anzats. Most often one uses atomic centered one-electron analytic functions to represent atomic orbitals (AOs), which are linearly combined into MOs

$$!_i = \sum_{\#} C_{\#i}\#_{\#} \qquad (2.7).$$

Using (2.5) one constructs the Roothaan-Hall equations[24]

$$\mathbf{FC} = \mathbf{SC} \qquad (2.8)$$

where **F** is the Fock matrix ($F_{\,!}=\%\#\,|\mathbf{F}(\,\&,\#)$ of different MOs, **S** the overlap matrix ($S_{\,!}=\%\#\,(\,\&,\#)$ between different basis functions, $\%$ is the diagonal MO energy matrix and **C** the matrix containing the MO expansion coefficients that needs to be determined. This is done in an iterative procedure, the so-called self-consistent field (SCF) approach. With this done one has derived the lowest possible energy of the system at hand, within the basis functions chosen. For the open-shell system the Pople-Nesbet equations have to be used to perform a SCF procedure on a UHF wavefunction.

So why use HF? Within the two approximations, the adiabatic and BO approximation, no further approximations are introduced and the electronic energy for a given set of nuclear positions will only depend on the set of basis functions used (basis set). A larger basis set will always give an energy closer to, but not lower than, the true energy of the system. However, even with an infinite basis set HF theory will not give the true energy for the system. HF will always overestimate the energy due to lack of electron-electron correlation. To enable a more exact energy calculation one must therefore go beyond the simple HF method.

2.1.2. Electron Correlation

In HF theory there are two types of electron-electron interaction, the exchange interaction and the Coulomb interaction. The exchange interaction, originating from the spin of the electrons, is a non-local effect and is treated

properly by use of the Slater determinant. The Coulomb interaction on the other hand is less well handled in HF theory. Since the electron only interacts with a mean field of the other electrons in the molecule, this approximation does not take into account the short distance interaction of two electrons, the so-called *dynamic correlation*.

Another problem that sometimes arises when using HF with one single determinant is that, for a given nuclear arrangement, two or more electronic states can be close in energy, displaying near-degeneracy effects. In such a case one needs to introduce *static correlation*, which technically is achieved by mixing of HF-states.

In a general sense one can construct an electron correlated wavefunction ! consisting of more than one SD, i.e. a linear combination of the HF (% $_{HF}$#) and excited SD (% $_i$#). In dynamically electron-correlated methods the HF wavefunction is the reference and the excited SDs are used as bases to describe the dynamical electron correlation.

$$\# = c_0 |! \ _{HF}\rangle + \sum_i c_i |! \ _i\rangle \qquad (2.9).$$

Here c are the coefficients giving the weight of each SD and ensuring that the wavefunction is normalized. The conceptually simplest electron correlated method is *configuration interaction* (CI). In a *full* CI (FCI) calculation the $_i$ are excited determinants, where one, two, three and up to n electrons are lifted from the occupied orbitals in the HF determinant and put into unoccupied orbitals (n is the number of electrons in the molecule). However, with increasing size of the molecular systems this method rapidly becomes impossible to handle as the number of SD to calculate becomes very large. There are simplifications to FCI, such as a truncated version of CI where only single and double excited determinants are used (CISD). The problem with the truncated CI is that the amount of electron correlation is dependent on the size of the system (size inconsistent), so comparison between molecules with different number of electrons cannot be made.

Static electron correlation

A molecule for which static electron correlation is important is best dealt with by *multi-configurational self-consistent field* (MCSCF) methods, i.e. methods in which the wavefunction is built up as a linear combination of SD's ($_i$), generally written as

$$\# = \sum_i c_i |! \ _i\rangle \qquad (2.10).$$

This is in contrast to CI where a HF wavefunction is used as the reference wavefunction. One type of MCSCF is the *complete active space* SCF (CASSCF) method, which is of special interest for this thesis. In the CASSCF method not only the coefficients in front of the SDs are computed but also the orbital coefficients within each SD. The determinants considered depend on the basis of the active space, which consists of the MOs that are considered to be of interest for the problem at hand. This active space of occupied and unoccupied orbitals is populated with a certain number of electrons (CAS(k,l)) and all possible excited determinants are formed. This can be a very large number as k electrons in l orbitals can form N number of determinants according to

$$N = \frac{l!(l+1)!}{\left(\frac{k}{2}\right)!\left(\frac{k}{2}+1\right)!(l-\frac{k}{2})!(l-\frac{m}{2}+1)!} \qquad (2.11).$$

For example, 12 electrons in an active space of 14 orbitals give 2 147 145 determinants. This number is reduced using spin and symmetry constraints since one specifies multiplicity and symmetry of the wavefunction in advance.

As the number of determinants rapidly grows with the size of active space, one cannot, except for very small molecules, include all electrons and orbitals in a CASSCF calculation. Thus, the choice of the active space becomes important. There is no automated method for this selection and instead one must manually inspect which orbitals and how many electrons are needed to give a proper description of the electronic states of interest. However, some guidelines can be used;

- k and l should generally be of the same size
- HF orbitals can give some insight into the orbitals of chemical relevance, and
- occupation numbers of natural orbitals[25] (NO) from MP2 or CISD calculations can indicate the importance of particular orbitals.

Still, benchmarking of the system at hand is crucial to ensure that the right active space has been selected. As a rule of thumb, NOs with occupation numbers less than 0.05 and greater than 1.95 are of less importance to the active space.

Dynamic electron correlation

If there are no problems with degenerate electronic states, or if the wavefunction already has taken that into account, there still is the problem of dynamic correlation. As mentioned in 2.1.1, in HF theory the Coulumbic interaction between electrons is only treated in an average fashion. To calculate a better energy the description of this interaction has to be improved and there

are several methods for this. Here, perturbation theory and coupled cluster theory (CC) will be described briefly. A conceptually different method is density functional theory (DFT) which will be discussed in chapter 2.2.

Perturbation theory

Perturbation theory can be applied to both to single- and multireference wavefunctions to treat dynamic electron correlation. Normally, perturbation theory on a single-reference wavefunction implies the so-called Møller-Plesset (MPn, n = 2, 3,…) method, where n represents the order of the perturbation expansion. In MPn methods the Hamiltonian $\mathbf{H}$ is composed of $\mathbf{H_0}$, with a known energy, and the perturbation operator $\hat{\mathbf{U}}$ with a variable parameter determining the strength of the perturbation,

$$\hat{\mathbf{H}} = \hat{\mathbf{H}}_0 + \hat{\mathbf{U}} \qquad (2.12)$$

where

$$\hat{\mathbf{H}}_0 = \sum_i^N \mathbf{F}_i \quad \text{and} \quad \hat{\mathbf{U}} = \sum_{i}^{occ}\sum_{i>j}^{occ} \frac{1}{r_{ij}} - \sum_{i}^{occ}\sum_{j}^{occ} \left(\mathbf{J}_{ij} - \frac{1}{2}\mathbf{K}_{ij} \right) \qquad (2.13).$$

The MPn wavefunction and energy of the system is then written as the zeroth order contribution plus corrections, written as Taylor expansions

$$\Psi = \Psi_0 + \lambda \Psi_1 + \lambda^2 \Psi_2 + \ldots \;, \; E = E_0 + \lambda E_1 + \lambda^2 E_2 + \ldots \qquad (2.14).$$

Excited SDs are used to construct the perturbation corrections. It can be shown that the zeroth order energy (E_0) is equal to the sum of orbital energies from a HF calculation and that the first order correction (E_1) is the HF energy. Thus, the second order perturbation theory (MP2) is the lowest order that includes a correction to the HF energy.

In the MP2 corrections to the energy, one can exclude the singly excited SDs because Brillouin's theorem tells that there is no coupling between singly excited determinants and the HF reference SD. In the formula for the MP2 energy correction only the doubly excited SDs remain, since the perturbation is a two-electron operator and all matrix elements with triple, quadruple etc excitations are zero. The expression for the MP2 energy correction written in MO basis then becomes

$$E(\mathrm{MP2}) = \sum_{i<j}^{occ}\sum_{a<b}^{vir} \frac{\left[\left\langle \phi_i \phi_j \middle| \phi_a \phi_b \right\rangle - \left\langle \phi_i \phi_j \middle| \phi_b \phi_a \right\rangle \right]^2}{\varepsilon_i + \varepsilon_j - \varepsilon_a - \varepsilon_b} \qquad (2.15).$$

The usage of MP*n* methods is rather straightforward and they are implemented in most quantum chemistry program code. Although an MP2 calculation recovers about 80% of the electron correlation energy and MP4(SDTQ), including single-, double-, triple and quadruple excitations, gives up to 95 - 98% of the correlation energy, there are some drawbacks. The variational principle is no longer valid once the MP*n* correction is added, and thus, the energy obtained can be below the true energy, which can be seen in an oscillatory behavior. Sometimes there is also a problem to project out spin-contaminations found in unrestricted calculations. These are seldom a practical problem, however, the scaling of computational cost is. The MP2 method scales as N^5 and MP4(SDQ) as N^6, where N is the number of basis functions. Memory and disc requirements also increase compared to an HF calculation.

Using perturbation theory on a multireferent wavefunction is more complicated as more than one SD describes the ground state wavefunction. In the CASPT2 approach the CASSCF wavefunction is taken as the reference, $_0$ in (2.14), and the Hamiltonian is constructed with only the single and double excited configurations included so that the first order wavefunction, as given in (2.14), is

$$\left|\,!\,_1\right\rangle = \sum_{p,q,r,s} C_{pqrs}\left|pqrs\right\rangle \qquad (2.16)$$

where *pqrs* gives the excitations of $\#\ _1!$ from *p* to *r* and from *q* to *s*. Further manipulation gives an expression for the coefficient matrix **C** containing the expansion coefficients as

$$\mathbf{C} = \mathbf{V}\left(\mathbf{F} \quad E_0\mathbf{S}\right)^{1} \qquad (2.17)$$

where **V** is the interaction between the zeroth order wavefunction and the excited configurations, **F** is the Fock matrix and, as the configurations do not have to be orthogonal, **S** is the overlap matrix.

Coupled Cluster Theory

A mathematically elegant way to estimate the electron correlation energy is through coupled-cluster theory. Here the electron-correlated coupled-cluster wavefunction $_{cc}$ is written as an exponential of a cluster operator acting on a single-reference HF wavefunction, i.e.

$$_{cc} = e^{\mathbf{T}}\ _{HF} \qquad (2.18).$$

The cluster operator **T** is divided into classes of single, double, triple excitations and so on

$$\mathbf{T} = \mathbf{T}_1 + \mathbf{T}_2 + \ldots + \mathbf{T}_n \qquad (2.19),$$

where n is the total number of electrons. When the $\mathbf{T}_i$ operator acts on the wavefunction it generates all possible determinants with i electrons excited from the reference HF wavefunction. As for example with $i = 2$,

$$\mathbf{T}_2 = \sum_{i<j}^{occ} \sum_{a<b}^{vir} t_{ij}^{ab} \, \mathbf{a}_{ij}^{ab} \qquad (2.20).$$

Here t_{ij}^{ab} are the amplitudes (coefficients) for the excited SD which are determined by the constraint in (2.18).

In practice, $\mathbf{T}$ is truncated as it is otherwise comparable to a full CI calculation and thus only applicable on very small systems. As an example, truncation of the $\mathbf{T}$ operator after second order gives

$$e^{\mathbf{T}_1+\mathbf{T}_2} = 1 + \mathbf{T}_1 + \left(\mathbf{T}_2 + \frac{\mathbf{T}_1^2}{2!}\right) + \left(\mathbf{T}_2\mathbf{T}_1 + \frac{\mathbf{T}_1^3}{3!}\right) + \left(\frac{\mathbf{T}_2^2}{2!} + \frac{\mathbf{T}_2\mathbf{T}_1^2}{2!} + \frac{\mathbf{T}_1^4}{4!}\right) + \cdots \qquad (2.21).$$

Here the higher excitations are represented by $\mathbf{T}_2\mathbf{T}_1$ or $\mathbf{T}_2{}^2$ terms etc.. The inclusion of higher excitations in the exponential expression makes the CC method size consistent, in contrast to the truncated CI methods.

After determining the cluster amplitudes t for all operators of a given order, the CC energy can be calculated as

$$E_{\mathrm{CC}} = \left\langle \mathrm{HF} \middle| \mathbf{H} e^{\mathbf{T}} \middle| \mathrm{HF} \right\rangle \qquad (2.22).$$

Although CC methods use single-reference HF wavefunctions, systems with multireference character can, in some cases, be treated with good accuracy. A method of testing the quality of the CC wavefunction is to perform T_1 diagnostics, given by

$$T_1 = \frac{|t_1|}{\sqrt{N}} \qquad (2.23).$$

Here, t_1 is the amplitude of the cluster operator for single excitations and N is the number of electrons. For a CC calculation including singles and double (CCSD) excitations, a value of $T_1 < 0.02$ is acceptable. There is a closely related variant of CC called *Brueckner* theory, where the SD is constructed so that the contributions of the single excitations are exactly zero, which leads to an improvement in the description of multiconfigurational mole-

cules. The lowest Brueckner theory level includes only double excitations (BD) and is a slight improvement of CCSD with about the same computational cost.

The drawback of the CC methods is that they are computationally demanding. With N being the number of basis functions, CCSD scales as N^6, and including triple excitations (CCSDT) as N^8. There are schemes for including disconnected triples corrections (CCSD(T)), which increases the accuracy without too much expense of computational cost.

2.2. Density Functional Theory Methods

A different approach to electronic structure calculation is *density functional theory* (DFT). Instead of deriving the energy from the wavefunction, the electron density ((**r**)) is used as the fundamental quantity. A major advantage is that the electron density is a function of three variables, compared to the 3n variables that are involved in a wavefunction calculation, where n is the number of electrons. The (**r**) also implicitly incorporates both exchange and correlation effects.

In chemistry, DFT has become increasingly more popular during the last 10 - 15 years as it has shown great potential to produce accurate results at a low computational cost. In practice, some approximations must be made to implement the theory and the result can differ depending on how these are made. Benchmarking is therefore required to estimate the accuracy for the particular system at hand.

DFT is based on the Hohenberg-Kohn (HK) theorems, which state that:

- Every observable can be written as a functional of the ground state electron density.
- The ground state density can be calculated, in principle exactly, using the variational principle involving only the density.

The problem is that the exact functional is unknown, so the challenge is to design a functional as accurate as possible. The Kohn-Sham (KS) equations take an artificial reference system of non-interacting electrons, which has exactly the same electron density as the real system of interacting electrons. The KS orbitals are then used to approximate the kinetic energy of the non-interacting system. The total energy of the system can then be written as

$$E[\ ] = T[\ ] + V[\ ] + J[\ ] + E_{xc}[\ ] \qquad (2.24)$$

where T is the kinetic energy, V is the electron-nuclear interaction, J takes care of the Coulomb repulsion and electron self-interaction, and E_{XC} is the exchange-correlation term, where all other contributions to the energy not

previously accounted for are included. The challenge in DFT is thus the approximation of the E_{XC} term.

2.2.1. Functionals

To date there is no systematic procedure to obtain the exact exchange-correlation functional. Usually the E_{XC} term is separated into two parts, one pure exchange part and one correlation part, E_X and E_C, respectively. A majority of the different functionals belongs to either the *local density* or *generalized gradient* approximation methods, LDA or GGA for short.

The density can be assumed to be local and thus be treated as a uniform electron gas. In most cases the density is divided into ( ) and (!) for the two spin densities, so-called *local spin density approximation* (LSDA), which gives the E_{XC} term the following expression

$$E_{XC}^{LSDA} = \&_{XC}\left[\%^{!}(\mathbf{r}),\%^{\#}(\mathbf{r})\right]\%(\mathbf{r})d^3\mathbf{r} \qquad (2.25)$$

where the integrand $\#_{XC}$ is sampled over the electron densities (**r**) and $^{!}$(**r**) at each point **r**. For a closed-shell system LSDA is equal to LDA. Despite the simplicity of the approximation in LSDA the accuracy is equal to that of the HF method.

To improve the LSDA one can look at the electron gas as a non-uniform gas. These methods assume that the functional not only depends on the local density but also on the gradient of the density. Such methods are called *generalized gradient approximation* (GGA) methods and the E_{XC} term then takes the following expression

$$E_{XC}^{GGA} = f_{XC}\left(\%^{!}(\mathbf{r}),\%^{\#}(\mathbf{r}),\left|\&\%^{!}(\mathbf{r})\right|,\left|\&\%^{\#}(\mathbf{r})\right|\right)d^3\mathbf{r} \qquad (2.26).$$

There are numerous gradient corrected functionals developed to give the correlation energy, one of the most commonly used being the functional proposed by Lee, Yang and Parr (LYP).[26]

In many cases the accuracy can be improved by generalizing the functional to be a combination of LSDA, GGA and also exact exchange as provided by HF. This leads to *hybrid methods*, functionals which in a general form can be written as

$$E_{XC}^{Hyb} = E_{XC}^{DFT} + a_0\left(E_X^{Exact} - E_X^{DFT}\right) \qquad (2.27).$$

Here the parameter a_0 allows for the description of the non-locality in the exchange-correlation hole. Becke has developed one of the most widely used

hybrid methods,[27] which later was combined to the functional known as B3LYP.[28]

2.3. Basis Sets

To approximate the molecular orbitals, a linear combination of basis functions (approximate atomic orbitals) is often used. They are used to build up wavefunctions in *ab initio* methods and describe the electron densities in DFT. The basis functions are mathematical functions chosen with some considerations in mind; they should make some chemical sense, be as few as possible and be easy to implement in a computationally efficient fashion.

The most commonly used basis functions are Slater type (STO) and Gaussian type (GTO) functions. Although STOs have a close resemblance to hydrogenic atomic orbitals, there is no analytical solution to the SCF procedure when they are used. If one uses GTO, about three times as many are required to resemble the shape of an STO, however, they are easier to implement computationally and are therefore preferred.

To generate GTOs with a good shape, linear combinations of primary GTOs (PGTO), i.e. contractions, are made. These contracted GTOs (CGTO) are made in two main different ways, *segmented* and *general* contractions. The latter uses all available PGTOs whereas the former uses a selection of the PGTOs for each contraction.

In order to better describe chemically relevant electrons one normally divides the basis functions into core and valence parts. To further introduce flexibility in the basis set the valence part is often divided further, so-called split valence basis set. Improvement of the basis set can be done, by augmentation of extra basis functions that describe polarization and/or diffuse characteristics of the electron distribution of an atom, which is important when the atom is included in a molecule.

A popular segmented contraction scheme is that of the Pople style basis sets where the CGTOs are fitted to STOs, such as the *6-31G(d)*. Whereas the core part in 6-31G(d) is built up by six PGTOs, the inner valence part contains three PGTOs and the outer part has one PGTO. The *G* stands for Gaussian-type functions and *(d)*, sometimes "*", tells that d-type polarization functions are added for elements heavier than hydrogen.

The general contraction scheme basis sets used in this thesis are the *atomic natural orbitals* (ANO) and the *correlation consistent* (cc-pV*n*Z, -*polarized Valence*, *n* = level of contraction, *Zeta*). These types of basis sets are used when a very accurate wavefunction is desired. The ANO basis set for an element is a general contraction chosen from a large set of PGTOs, which are NOs that diagonalize the density matrix. In this way the basis set size is determined by how many PGTOs to include, i.e. a basis set for Si can be written as [4s3p1d] and it is a subset of the [5s4p2d] basis set, where the

latter has one additional PGTO of each type. The cc-pV*n*Z type basis sets use a smaller selection of PGTO than the ANO and are optimized to recover as much as possible of the electron correlation energy of the valence electrons. The *n* in the acronym refers to the number of contractions, e.g. *D* = double, *T* = triple, *Q* = quadruple. The disadvantage of ANO and cc-pV*n*Z basis sets is that they are computationally demanding, the former more so than the latter, and they are therefore only used when high accuracy is desired.

To better describe properties other than the energy of a molecule it is sometimes necessary to use basis sets derived for one particular property. Such can be the case if one wants to determine the polarizability with a high accuracy. For this purpose Spackman developed a set of auxiliary polarization and diffuse basis functions to the 6-31G basis set,[29] which have the advantage that there is only a minor additional computational cost added. This basis set is written as 6-31(+sd+sp). For an even better description, Sadlej developed a complete basis set optimized for polarizability calculations, often referred to as *POL* basis set,[30] which is larger than the former by Spackman and is therefore mostly used on smaller systems.

2.3.1. Effective Core Potentials

For heavier elements in the periodic table, i.e. from the third row and down, the number of core electrons per atom increases to the extent that they severely affect the computational cost. For the bottom half of the elements in the periodic table the electrons closest to the nuclei will also be influenced by relativistic effects. Since the core electrons from a chemical point of view are uninteresting, one way to bypass these two issues is to use an *effective core potential* (ECP), also called *pseudopotential*, where the core electrons are replaced by a semi-empirically derived potential and only the valence electrons are treated explicitly by basis functions. In this thesis two different ECPs have been employed, one double-zeta ECP developed by Los Alamos National Laboratory (LANL2DZ) and a larger Stuttgart–Dresden–Bonn (SDB) ECP, [31,32] the latter developed to work in conjunction with the cc-pVTZ basis set. The LANL2DZ can also be extended with the diffuse- and polarization basis functions developed by Sunderlin and co-workers,[33] abbreviated LANL2DZdp.

3. Ring Strain Calculations

To predict the difficulty of making a novel compound there are several factors that need to be taken into account. For cyclic compounds the strain that stems from forming one or several rings is one factor that influences the stability. But also factors such as reactivity towards other compounds, for example water, acid or base are important. For the novel class of bicyclic compounds studied in this thesis the ring strain was considered to be one of the important factors to investigate, and to estimate their ring strains a number of methods can be used.

3.1. Homodesmotic Reactions

The destabilizing ring strain of a cyclic molecule cannot be obtained from one single *ab initio* or DFT calculation since there is no operator for this quantity. Instead one must compose a hypothetical reaction where the energy of the cyclic compound is related to that of one or more open-chain compounds. One of the simplest ways is an *isodesmic reaction*, *Figure 11a*, where the number of bonds between heavy atoms (atom number > 1) are equal on both sides of the equation.[34] However, the studies in this thesis use the *homodesmotic reaction* scheme,[35] where also the hybridization states of the heavy atoms are equal on both sides of the reaction, and the various types of heavy atom-hydrogen bonds are matched as closely as possible, *Figure 11b*.

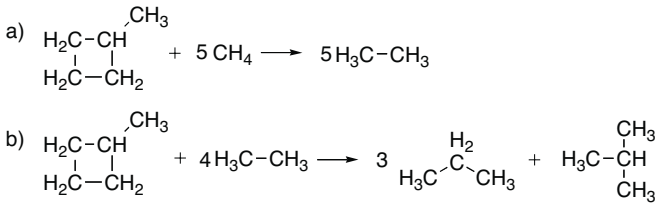

Figure 11. Example of reactions for the calculation of the ring strain of methylcyclobutane; a) an isodesmic reaction and b) a homodesmotic reaction.

The calculated ring strain is obtained by subtracting the total energy of the molecules on the r.h.s. from the total energy of the molecules on the l.h.s.

3.2. Heavy Group 14 1,(*n*+2)-Dimetallabicyclo[*n.n.n*]-alkanes, Propellanes and Related Compounds

With regard to synthetic realizability of the all-carbon compounds, **1a** - **6a** in *Figure 12*, they have all been synthesized and characterized, but their stabilities vary greatly.[36,37,38,39,40,41] The all-C bicyclo[*n.n.n*]alkanes (**1a**, **3a** and **5a**) and the [3.3.3]propellane (**6a**) are found to be inert, but most [2.2.2]- and [1.1.1]propellanes polymerize and/or rearrange with the inverted central C-C bond as the source of instability. The exception is the fluorinated [2.2.2]propellanes of the Lemal group, which display lower reactivity.[42]

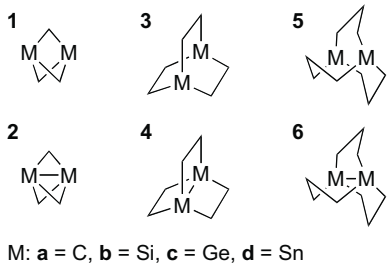

Figure 12. Structures for which rings strain energies were investigated.

One could reason that if a heavy dimetalla[*n.n.n*]propellane or dimetallabicyclo[*n.n.n*]alkane is less ring strained than its all-C analogue, it will be at least equally stable as the latter. The stabilities of the previously formed bicyclo[1.1.1]pentasilane,[43] bicyclo[1.1.1]pentastannane,[44,45] as well as 2,4,5-trithia- and 2,4,5-triselena-1,3-disilabicyclo[1.1.1]pentanes,[46] suggests that **1b** – **1d** have potential to be thermally stable at ambient temperatures.

Of other structurally related systems, Kira and co-workers in 2001 formed the first 1,3-disilabicyclo[1.1.0]butane, a compound with a partially inverted Si-Si bond, which also showed thermal stability even though it was sensitive to oxygen and moisture.[47] A fully inverted Si-Si bond is found in 1,3-disila-[1.1.1]propellane (**2b**), a species that so far has not been made, even though the parent all-carbon [1.1.1]propellane and a pentatanna[1.1.1]-propellane derivative, i.e. ligand-stabilized cluster compounds with "naked" Group 14 atoms, were formed by Wiberg and Walker and Sita *et al.*[48,44] Of larger synthesized [*n.n.n*]propellanes, only 3,7,10-trichalcogena-octasila[3.3.3]-propellanes and a 1,6-disila[4.4.4]propellane have heavy Group 14 elements in bridgehead positions.[49,50]

Ring strain and other properties have now been analyzed by computations, with the aim to rationalize which species can possibly exist at ambient temperatures.

3.2.1. Computational Ring Strain Results

As there are no experimental data for any of the heavier Group 14 substituted systems in this study, benchmark calculations were performed on the smallest systems, i.e. **1** and **2**. High-level calculations at CCSD(T)/cc-pVTZ(SDB) level on MP2/cc-pVTZ geometries where compared with MP2/cc-pVTZ(SDB), MP2/6-31G(d)(LANL2DZp) and B3LYP/cc-pVTZ (SDB) calculations. They showed that with ZPE corrections both the CCSD(T) and MP2 levels were in good agreement with the experimental results found in literature for compounds **1a** and **2a**. B3LYP underestimated the ring strain by about 5 and 10 kcal/mol for systems **1** and **2**, respectively, although the same trends within each compound class were seen. Optimized geometries are very similar at the MP2 and B3LYP levels, but with the former being slightly closer to experimental electron diffraction data.

Even though bicyclo[1.1.1]pentane (**1a**) is highly strained, 66.6 kcal/mol experimentally,[51] this compound is thermally stable until 300 ºC, above which it rearranges to 1,4-pentadiene.[37] The calculations reveal that 1,3-dimetallabicyclo[1.1.1]pentanes (**1b** - **1d**) are less strained than **1a** by 12 - 15 kcal/mol, Table 1.

Table 1. *Calculated homodesmotic ring strain energies at MP2/6-31G(d) (LANL2DZp) level, normal text, with ZPE* corrections in italics and CCSD(T)/cc-pVTZ with ZPE* in parenthesis.*

Compound	HDE / kcal mol^{-1}	Compound	HDE / kcal mol^{-1}
1a	70.2, *65.2*, (64.9)	**2a**	104.0, *96.0*
1b	55.4	**2b**	77.9
1c	55.4	**2c**	63.7
1d	54.2	**2d**	55.3
3a	10.8	**4a**	102.0
3b	13.2	**4b**	87.6
3c	16.0	**4c**	77.4
3d	17.8	**4d**	65.5
5a	23.6	**6a**	13.6
5b	11.5	**6b**	35.2
5c	10.3	**6c**	39.4
5d	8.5	**6d**	51.4

* ZPE corrections at MP2/6-31G(d) level.

These compounds should thus be thermally stable at ambient temperature, similarly as concluded by Allen and co-workers for **1b**.[52] The stability of the related compounds mentioned above, [43,44,45,46] also support this conclusion. In the case of **1b** - **1d** the electron density is drained from the bridgehead M atoms, due to their lower electronegativity. These atoms have then an increased electrophilicity, and are potentially vulnerable to attack by nucleophiles. Transition states for attack of H_2O to these sites with simultaneous breakage of the M-C bonds leading to 1,3-dimetallacyclobutanes were lo-

cated. At the MP2/6-31G(d)(LANL2DZp) level the transition states are found at energies 27.0 (**1b**), 25.6 (**1c**) and 14.0 (**1d**) kcal/mol relative to reactants, and at B3LYP level these energies are 22.3 (**1b**), 20.4 (**1c**) and 10.1 (**1d**) kcal/mol. The barriers will likely be lower if several H_2O molecules assist in the M-C bond breakage. This indicates that **1d** will rapidly degrade when exposed to moisture, whereas **1b** and **1c** will have longer lifetimes, but presumably also slowly degrade upon exposure to moisture.

An interesting geometrical feature of systems **1a** and **1b** are the $M_{bh}\cdots M_{bh}$ distances. For **1a** the distance is longer than the C-C bond in ethane, but for **1b-d** they are almost equal or shorter than the corresponding $H_3M\text{-}MH_3$ bond lengths, *Figure 13*.

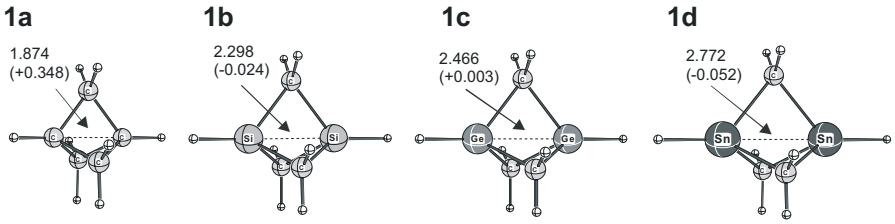

Figure 13. Optimized structures of **1a-d** with inter-bridgehead distances and differences to corresponding $H_3M\text{-}MH_3$ bond lengths in parentheses, calculated at MP2/6-31G(d)(LANL2DZp) level.

These relatively short distances suggest that a stronger through-space coupling could be seen, as the bridgehead atoms become heavier.

Similar as for **1**, changing the bridgehead atoms in **2** from C to Si, Ge or Sn lowers the strain energy, Table 1. Since [1.1.1]propellane (**2a**) exists in the gas phase until 114 °C and in solution until 0 °C, [36,53,54] it is tempting to reason that the 1,3-dimetalla[1.1.1]propellanes (**2b** – **2d**) may be equally stable. However, this argumentation overlooks the increased M-M bond polarizability of the propellanes as one descends the group which should promote oligomerization. This is critical for 1,3-dimetalla[1.1.1]propellanes where the M···M distances in analogous dimetalla-[1.1.1]propellanes and dimetallabicyclo[1.1.1]pentanes are similar when M = Si - Sn. CASSCF(4,4)/6-31G(d) calculations on the formation of dimeric biradicals from **2a** and **2b** reveal essential differences in their first oligomerization steps. In **2a**, the $C_{bh}\text{-}C_{bh}$ bond has a bond order of 0.7,[55] and formation of the biradical dimer is thermodynamically unfavorable. In contrast, the Si-Si bond electron density in **2b** is diffuse and easily polarized, and this compound is neither thermodynamically nor kinetically stable toward dimerization as there is almost no barrier for this process. Because of less relief in strain from the dimerizations of **2c** and **2d** than of **2b**, the biradical dimers of these compounds are less stable than two monomers, but **2c** and **2d** should still be more prone to oligomerize than **2a**.

In contrast to the 1,3-dimetallabicyclo[1.1.1]pentanes, a very modest strain increase accompanies the change of bridgehead element from C to Sn in 1,4-dimetallabicyclo[2.2.2]octanes (**3**), Table 1. However, overall **3a** - **3d** are much less strained than their smaller analogues, and judged from the strain these species should be thermally persistent when generated. They are structurally similar to group 14 9,10-dimetallatriptycenes,[56,57] compounds that are formed and handled by standard laboratory techniques. The M···M distances for **3a**-**d** are longer by approximately 1.06, 0.65, 0.65 and 0.50 Å when compared to the M-M bond lengths of H_3M-MH_3 species, and thereby shorter than the sum of the van der Waals radii.[58] The modest increase in strain could possibly be caused by larger eclipsing strain between the M-C bonds when descending Group 14, as the ethylene linking bridges become more twisted, less eclipsed, when going from **3b** to **3d**, *Figure 14*.

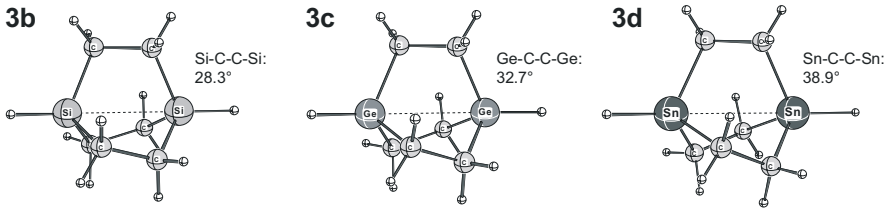

Figure 14. Optimized structures of **3b-d** with M-C-C-M dihedral angles of the ethylene bridges, calculated at MP2/6-31G(d)(LANL2DZp) level.

Comparing the 1,4-dimetalla[2.2.2]propellanes **4a** to **4d**, the major difference between them is that **4a** is a closed-shell species whereas **4b** – **4d** are biradicals without M-M bonds. The strain in the closed-shell M-M bonded structures of **4b** – **4d** are apparently larger than the M-M bond strengths. With ethyl tethers, there is a mismatch between the tether and the optimal M-M bond length. So for **4b** – **4d** the strengths of the M-M bonds do not compensate the high strain imposed by the tethers at closed-shell M-M bonded structures.

As seen in Table 1, bicyclo[3.3.3]undecanes **(5a**) is the most strained of the 1,5-dimetallabicyclo[3.3.3]undecanes (**5**) and earlier heat of formation measurements support its elevated strain.[59] The heavier analogues are only half or even less as strained, and the heavier congeners **5b**-**d** should all be synthetically feasible. The trend in strain energy when descending the group is thus different from that in 1,4-dimetallabicyclo[2.2.2]octanes, and the reason for the particular strain in **5a** can be found in the C-C-C angles of the tethers. These are almost 120°, whereas they are closer to tetrahedral (109.5°) in **5b** – **5d** (114 – 116°).

For the 1,5-dimetalla[3.3.3]propellanes (**6**) the mismatch between optimal M-M bond and tether lengths becomes larger as one descends the group; the M atoms go from sp^3 to sp^2 hybridization and the M-M bonds gradually shorten, *Figure 15*.

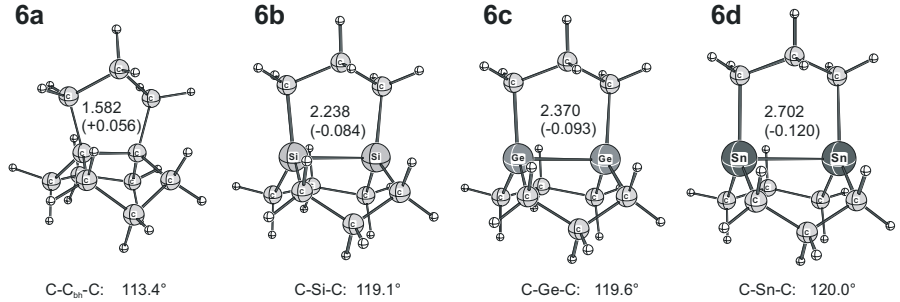

Figure 15. Optimized structures of **6a**-**d** with inter-bridgehead distances and difference to corresponding H_3M-MH_3 bond lengths in parentheses as well as tether valence angles calculated at MP2/6-31G(d)(LANL2DZp) level.

This can be seen in the increase in ring strain with heavier group 14 element in the bridgehead position, Table 1. The homolytic Sn-Sn bond dissociation energy of **6d** is low as a result of the inverted character of this bond, and this compound will rapidly oligomerize. Only propellane **6b** should be truly persistent at ambient temperature and it is most likely also not reactive to moisture.

Heteroatom bridges

In search for other compounds structurally similar to 1,3-dimetallabicyclo[1.1.1]pentane, the methylene bridges were replaced with other functional groups or elements. Several combinations have been investigated, *Figure 16*, and the goal was to probe if any of these compounds display a reasonably low ring strain and at the same time have the bridgehead atoms at short distance.

M = Si, Ge, Sn:
X = CH_2 (**7**), CMe_2 (**8**), NMe(**9**),
O (**10**), MMe_2 (**11**), PMe (**12**), S (**13**).

M = Si:
X = $C(CMe_3)_2$ (**14**), $C(CH_2)_nCH_2$
n = 1 (**15**), 2 (**16**), 3 (**17**).

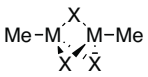

M = Si, Ge, Sn.
X = MMe_2 (**18**), PMe (**19**), S (**20**).

Figure 16. 1,3-Dimetallabicyclo[1.1.1]pentane systems with heteroatom bridges.

It was concluded that compounds with aza and oxa bridges increase the ring strain compared to systems with only methylene bridges. The contrary was found for systems with all bridges consisting of MMe_2 or PMe, which have ring strain values between 29 and 39 kcal/mol at MP2/LANL2DZp level. In addition to lowered strain, the phospha bridge gives through-space distances between the bridgehead M atoms which are merely 6 – 10 % longer than normal M-M single bonds, *Figure 17*.

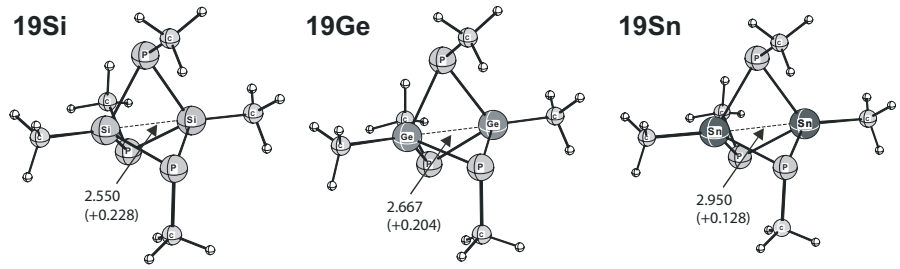

Figure 17. Optimized structures of **19Si, 19Ge** and **19Sn** with inter-bridgehead distances and difference to corresponding $H_3M\text{-}MH_3$ bond lengths in parentheses, calculated at MP2/(LANL2DZp) level.

In this context, it is worth noticing that two 1,3-distanna-2,4,5-triphosphabicyclo[1.1.1]pentanes (**19Sn**) have previously been reported in the literature. Experimental data of Schumann and Benda reports a melting point between 133 – 135 °C for one derivative whereas the other melted and degraded at 89 – 91 °C.[60] Both of these species were air sensitive. Recently, Wright and co-workers generated the dianion $[Sn_2(\ \text{-}PMes)_3]^{2-}$ with strong resemblance to **19Sn**.[61]

3.2.2. Synopsis

A selection of compounds presented in this chapter are considered by us as realistic synthetic targets, when based on ring strain energies, polymerization aptitude and water reactivity. However, these compounds may still be synthetically challenging due to intrinsic difficulties in their preparations, e.g. low stability of intermediates.

4. Theory and Calculation of Static Dipole Polarizabilities

4.1. Theory of Static Dipole Polarizability

The static electric dipole polarizability, , of a molecule is a measure of its ability to respond to an electric field, and either acquire an electric dipole moment or change its dipole moment. It can be related to the energy change of a molecule subjected to an electric field. The energy E of a charge distribution in an electric field can be written as a multipole expansion,

$$E = qV \quad \#\mathbf{F} \quad \frac{1}{2}\mathbf{QF}! \tag{4.1}$$

where q is the net charge, V the potential, the electric dipole moment, $\mathbf{Q}$ the quadrupole moment, $\mathbf{F}$ the electric field and $\mathbf{F}'$ the gradient of the field. In the presence of a homogenous electric field the induced dipole moment $_z$, in a given direction z, is given by

$$\%_z = \%_{0z} + \quad _{zz}F_z + \frac{1}{2}!_{zzz}F_z^{\,2} + \ldots \tag{4.2}$$

where $_{0z}$ is the permanent dipole moment, $_{zz}$ is the second rank polarizability tensor component and $!_{zzz}$ the third rank hyperpolarizability tensor component, in the z direction. The energy of the molecule in the presence of an electric field can also be written as a Taylor expansion,

$$E(\mathbf{F}) = E(0) + \left(\frac{!E\%}{\#\mathbf{F}\&}\right)_0\mathbf{F} + \frac{1}{2}\left(\frac{!^2E\%}{\#\mathbf{F}^2\&}\right)_0\mathbf{F}^2 + \frac{1}{3!}\left(\frac{!^3E\%}{\#\mathbf{F}^3\&}\right)_0\mathbf{F}^3 + \ldots \tag{4.3}.$$

Comparing the expression above with (4.2) inserted in (4.1) shows that the first derivative at zero field strength is the permanent dipole moment, the second derivative is the polarizability and the third derivative is the first hyperpolarizability. Equation (4.1) can therefore be written as

$$E(F_z) = E(0) \quad \%_{0z}F_z \quad \frac{1}{2}!\ _{zz}F_z^2 \quad \frac{1}{3!}\#_{zzz}F_z^3 + \ldots \qquad (4.4).$$

The equations (4.2) – (4.4) are restricted to the *z* direction, e.g. the polarizability along the z-axis in a cartesian coordinate system, *Figure 18*. This description will be taken as the principal axis of an oligomer. In case of a conjugated oligomer the longitudinal polarizability component $_{zz}$ will thus describe the polarizability in the direction of the conjugation.

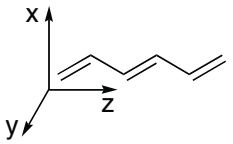

Figure 18. Definition of longitudinal axis as the z-axis.

The *average polarizability*, $_{avg}$, of a molecule is obtained as the trace of the polarization tensor divided by three, i.e.

$$_{avg} = \frac{1}{3}\ _{tr} = \frac{1}{3}\left(\ _{xx} + \ _{yy} + \ _{zz}\right) \qquad (4.5).$$

To compute the polarizability of a molecule is a question of calculating the second derivative of the energy at zero field strength. This can be done in several different ways. One way is to calculate the polarizability analytically using the coupled perturbed HF/KS scheme (CPHF/CPKS).[62] By using the fact that the HF wavefunction obeys the Hellman-Feynman theorem, an expression for the polarizability can be written as

$$\# = \frac{^2E_{HF}}{F^2} = 2\left\langle \frac{!\ _0}{F}\middle|\mathbf{r}\middle|!\ _0 \right\rangle \qquad (4.?).$$

To calculate the polarizability, the first derivative of the wavefunction with respect to the electric field is needed. The CPHF scheme introduces a perturbation to the HF equation and solves this perturbed HF equation in an iterative fashion. The CPHF/CPKS technique is available for single reference-methods, i.e. HF, MP2 and DFT.

Another approach is the *finite field* (FF) method where the second derivative is approximated as

$$\#_{zz} = \frac{\%^2E(}{+\ \&F_z^2\ )_0} = \frac{\left(2E(0)\ !\ E(F_z)\ !\ E(!F_z)\right)}{F_z^2} \qquad (4.6).$$

The FF approach can be used for any method since it only requires that the energy can be calculated with an applied electrical field taken into consideration. In this thesis the FF approach is used for MP2 and CCSD(T) methods. There are some caveats to mention in connection with finite field polarizability calculations. First, when the applied field strength is very small the energy difference in the numerator becomes so small that numerical noise in the calculation affects the result. To minimize this error the convergence criteria for the SCF procedure needs to be tightened, preferably down to 10^{-12} a.u..[63] On the other hand, if the electric field strength applied in the calculation is strong, higher order terms in the Taylor expansion eq. (4.4) can contribute significantly to the energy $E(\pm\mathbf{F}_z)$. To reduce their contribution, polarizabilities at different field strengths are calculated, and a quadratic fit of these points provides an estimate of the polarizability at zero field strength.[63]

4.2. Polarizability, Band Gap and Conjugation

In early attempts to estimate molecular polarizability, individual bond polarizabilities were used together with shape and size measurements of the molecule.[64] However, this model failed when applied to long-chain !-conjugated compounds. In the early fifties, Davies thus worked out a simple Hückel model for the longitudinal polarizability of !-conjugated carbon chains.[65] With this model he concluded that the longitudinal polarizabilities of such molecules depend on the cube of their lengths. However, for real !-conjugated compounds the dependence of longitudinal polarizability is lower as the model does not take factors such as bond length alternation into account. On the other hand, for non-conjugated systems the length dependence can be reasonably well described as a sum of independent polarizabilities of separated components. This was exemplified by Ghanty and Ghosh who revealed a linear dependence of the polarizability of water clusters on the number of water molecules.[66]

The power dependence of the longitudinal polarizability of conjugated compounds decreases with the length of the system and eventually the oligomer will reach a length above which the &$_{zz}$ increases linearly. The estimate of &$_{zz}$ per repeat unit is calculated from a plot of polarizability (&$_{zz}$ or #&$_{zz}$ against number of monomer units n, where

$$\bar{}_{zz} = \left({}^{n}_{zz} / n \right) \quad \text{and} \quad \#_{zz} = \left(\#^{n}_{zz} \,!\, \#^{n!1}_{zz} \right) \tag{4.7}$$

and &$_{zz}^{n}$ is the longitudinal polarizability for the oligomer consisting of n monomer units. The limiting value (n %) is obtained from extrapolation. Both of the (&$_{zz}$ or #&$_{zz}$ extrapolate to the same result, although #&$_{zz}$ converges faster as it is less compromised by end-effects, whereas the former is

less affected by numerical errors.[67] There are varieties of extrapolation techniques; from a simple fit to an exponential function to more complicated mathematically motivated nonlinear sequence transformations. The one chosen in this work is a simple fit of data points to an inverse polynomial as

$$\#_{zz}(n) = \sum_{i=0}^{i_{\max}} a_i n^{!\,i} \qquad (4.8).$$

Here $i_{\max}$ is the number of data points and a_0 becomes the limiting value corresponding to the polarizability per monomer unit in an infinitely long polymer chain, $\%_{zz}$ or $\#\%_{zz}$, depending on dataset used. The former tends to result in an underestimation of the infinite value and the latter is motivated when greater stability is needed.[67] From $\#\%_{zz}$ the conjugation length can be estimated, and it can be defined as the length where $\#\%_{zz}$ has reached 95 % of $\#\%_{zz}$. This property is also known as the saturation length $n_{0.95}$.

Yet another property that reflects the conjugation in a system is the ratio $\%_{zz}/\%_{avg}$ at infinite length. This ratio will approach three for a one-dimensional and perfectly conjugated polymer chain.

The band gap E_g is defined as the energy difference between the valence band and the conduction band of a compound. In the case of a single molecule it becomes the difference between the energy of the highest occupied MO (HOMO) and the lowest unoccupied MO (LUMO) and it can be estimated from the KS orbital energies, even tough it is slightly underestimated this way.[68]

4.3. Polarizabilities of Heavy-Core Staffanes

The properties of staffanes were briefly described in the introduction, here we investigate the polarizabilities and band gaps of heavy-core staffanes and compare them to those of known ! - and &-conjugated compounds.

Benchmark calculations of a number of small molecules with experimentally determined polarizabilities showed that both finite-field MP2 (FF-MP2) and CPHF calculations with the PBE0 functional together with either the POL or 6-31G(+sd+sp) basis set give satisfactory results. For staffanes and Si-core staffanes with $n \leq 4$ there is a very small difference between the FF-MP2 and the PBE0 results calculated with the 6-31G(+sd+sp) basis set, Table 2. This would indicate that the DFT in general and PBE0 in particular is a suitable method for estimating static polarizabilities, as also previously reported.[69]

Table 2. *Longitudinal polarizabilities of [n]staffanes and Si-core [n]staffanes calculated with FF-MP2 and PBE0 methods and the 6-31G(+sd+sp) basis set.*[*]

	All-C [*n*]staffane		Si-core [*n*]staffane	
n	FF-MP2	PBE0	FF-MP2	PBE0
1	54.3	53.3	100.3	98.9
2	120.2	118.4	276.8	265.8
3	193.7	191.2	474.2	473.9
4	271.0	267.8	700.9	704.1

* Polarizabilities in a.u.

However, for longer conjugated molecules we found that, in general, the PBE0 functional exaggerates the absolute value of the longitudinal polarizability compared to HF values, Table 3, and to previously reported values for oligothiophene calculated with MP2 using the CPHF wavefunction.[70] Subsequently, the PBE0 functional will be used to calculate a qualitative trend (*vide infra*) of the polarizabilities of the all-C and heavy-core [*n*]staffane with $n \leq 15$, while HF calculations possibly will represent a closer agreement to other high-level calculations. For longer systems, $5 \leq n \leq 15$, a smaller basis set needed to be used, and for heavier elements an ECP is also required. Earlier studies showed that the longitudinal polarizability is less dependent on basis set than the average polarizability,[71,72] which also were our finding with 6-31G(d) and LANL2DZp when applied to the all-C and Si-core staffanes.

A set of polarizability calculations with the 6-31G(+sd+sp) basis set were performed on short all-C and Si-core [*n*]staffanes, as well as on oligomers with three other conjugation topologies. These were either rigid -conjugated, [*n*]acenes and [*n*]cumulenes, or conventionally #-conjugated, permethylated oligosilanes, *Figure 19*.

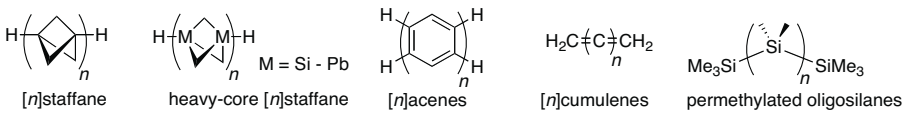

Figure 19. Compound classes in polarizability calculations of short oligomers.

The choice of the two -conjugated systems was done based on rigidity, since their conjugations cannot be attenuated by conformational twists. However, oligosilanes are conformationally flexible, but in our calculations the Si backbone conformation was restricted to the all-anti conformer,[73] with the backbone dihedral angles set to 180º.

The power dependence, ! , of $_{zz}$ to length was derived through a fit of the data points to the function $_{zz} = aL^{!}$, where L is the length of the molecule.

For staffanes with $n \leq 4$, the $\#_{zz}$ of all-C staffanes has a length dependence of %= 1.29, but Si-core staffanes up to the same number of monomer units reach a value of %= 1.52 at PBE0/6-31G(+sd+sp) level. With regard to the cumulenes, acenes and oligosilanes they all have higher exponents of the fitted curves; 1.71, 1.86 and 1.62, respectively, which gives perspective on what power dependence to expect from traditionally conjugated molecules. The nonlinear dependence of the longitudinal polarizability on length was earlier calculated for the parent oligosilanes, and taken as a clear indicator of &-conjugation.[74] This gives a strong indication that a step down Group 14 from C to Si as bridgehead element, i.e. a Si-core, the staffanes show increased nonlinear behavior typical for a conjugated system. This trend is clearly seen as calculations with the 6-31G(d) basis set and LANL2DZp ECP for all-C and heavy-core [*n*]staffanes until $n = 4$, give power dependencies of %= 1.19 (C), 1.42 (Si), 1.50 (Ge), 1.61 (Sn), and 1.90 (Pb) at PBE0 level.

The calculations of $\langle\#_{zz}$ or $!\#_{zz}$ were not only performed for the all-C and heavy-core staffanes, but also for heavy alkanes, oligopyrroles and oligothiophenes, the latter two being thoroughly investigated oligomers with regard to polarizability as well as conductivity.[75,76] The expected faster convergence for the $!\#_{zz}$ compared to $\langle\#_{zz}$ is seen in *Figure 20* as well as some signs of instability of $!\#_{zz}$ values for Pb-core staffanes can be noted.

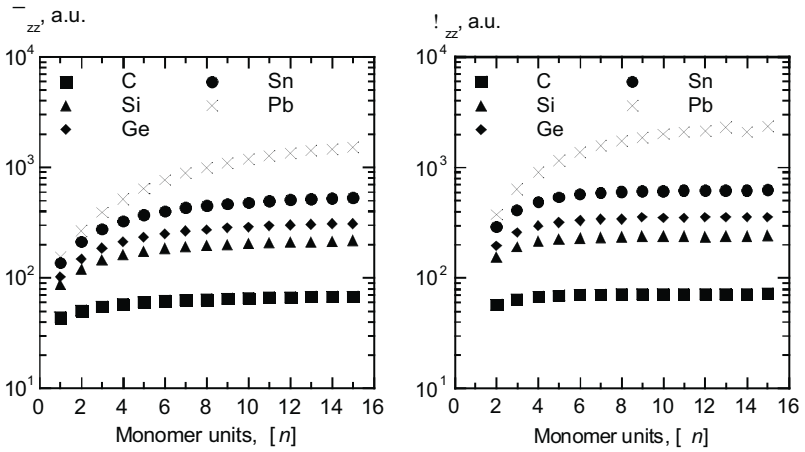

Figure 20. Variation of $\langle\#_{zz}$ (left) and $!_{zz}$ (right) with *n* calculated at PBE0//PBE0 level for all-C and heavy-core [*n*]staffanes using 6-31G(d) for all-C and LANL2DZp for Si/Ge/Sn/Pb-core staffanes.

The trend for the heavy-core staffanes of increasing $\langle\#_{zz}$ and $!\#_{zz}$ when going down group 14 is evident. The largest increases are found when changing the bridgehead element from C to Si and from Sn to Pb, *Figure 20*.

The differences between estimated α_{zz} and $\langle \alpha_{zz} \rangle$ are small in all the calculated systems, except for the Pb-core staffanes, Table 3. Although the values for the Pb-systems cannot be approximated to any precision, the high longitudinal polarizability indicates a nearly perfect conjugation.

Table 3. *Limiting polarizability and band gap values when* $n \to \infty$ *for all-C and heavy-core [n]staffane polymers as well as polythiophene, polypyrrole and polysilane at PBE0//PBE0 and HF//PBE0 level.*[*]

Polymer	α_{zz}^{∞}		$\langle \alpha_{zz} \rangle^{\infty}$		$(\alpha_{zz}/\alpha_{avg})^{\infty}$		E_g^{∞}
	PBE0	HF	PBE0	HF	PBE0	HF	PBE0
all-C [*n*]staffane	71.9	64.8	71.8	65.1	1.43	1.36	9.74
Si-core [*n*]staffane	243.1	181.1	240.7	182.0	2.03	1.85	4.76
Ge-core [*n*]staffane	357.4	262.9	355.1	266.5	2.21	2.03	4.59
Sn-core [*n*]staffane	638.8	430.1	632.3	431.2	2.42	2.23	3.32
Pb-core [*n*]staffane	(2505.4)	(1254.5)	(3129.3)	(1314.3)	2.87	2.68	1.44
Polythiophene	415.2	250.9	407.6	248.3	2.49	2.33	2.24
Polypyrrole	217.0	156.20	220.3	165.0	2.38	2.19	3.10
$H(SiH_2)_nH$	142.8	105.5	145.6	106.9	1.96	1.77	5.10

* Polarizabilities in a.u. and band gaps in eV. The 6-31G(d) basis set was used for the all-C staffanes and polypyrroles, and the LANL2DZp ECP for the Si/Ge/Sn/Pb-core staffanes, polythiophenes and polysilanes. Limiting values derived by inverse polynomials.

The conjugation lengths in number of units estimated from $n_{0.95}(\langle \alpha_{zz} \rangle)$ for heavy-core staffanes increase as the bridgehead element gets heavier, from 4.5 for the all-C to over 15 for Pb-core staffanes. Polythiophene and polypyrrole values are 12.4 and 9.9, respectively, which is just slightly higher than that of Sn-core staffanes at 8.5.

Regarding the α_{zz}/α_{avg} ratio for the heavy-core staffanes the trend is, not surprisingly, the same as for limiting polarizabilities, i.e. the ratio increases down Group 14, Table 3. All the heavy-core staffanes have a ratio equal or higher than that of polysilanes, for which Jansik *et al.* previously reported a value of 1.9,[77] which agrees well with our findings. However, the backbones of polysilanes adopt a zigzag shape and the polarization will therefore to some degree be directed perpendicular to the z-axis, giving a lower α_{zz}/α_{avg} ratio. Again, the Sn-core staffane has a value at infinite length close to that of polythiophenes and polypyrroles.

With regard to the calculated absolute values of the polarizability there is a large difference between HF and PBE0. This issue has not been addressed within this work and needs further investigation. For small molecules and short conjugated oligomers the polarizabilities obtained with the PBE0

method agrees well with experiments and those obtained at MP2 level. In contrast, for longer oligomers the PBE0 values are overestimated by as much as a factor of two compared to reported MP2 calculations. This is symptomatic also for other DFT functionals benchmarked, and the results are not significantly improved by a better basis set. One can only speculate about the origin of this error at the moment. Adamo and co-workers recently found that geometrical properties of conjugated oligomers are poorly described due to the the self-interaction correction error, an inherent problem in all DFT functionals.[78,79]

The estimated band gaps for staffanes range from 9.74 eV for the all-C to approximately 1.4 eV for the Pb-core staffane. Once again, the largest change is when replacing C by Si in the bridgehead position in the staffanes. The Si-core staffane has a band gap in comparable size to the polysilanes, whereas the Sn-core is in the same range as for polypyrrole. The trend for band gaps follows those of α_{zz} and β_{zz}. If the band gaps calculated at B3LYP/LANL2DZp are compared with experimentally determined values for polythiophene and polypyrrole, 2.5 and 3.2 eV, [80, 81] respectively, the computationally predicted values are in good agreement.

4.4. Synopsis

From the calculated results the conclusion can be made that heavier Group 14 elements in the bridgehead position increase the polarizability, increase the conjugation as judged from the Hückel type model and reduce the band gaps. The values for the Sn-core staffanes are in the same range as those of polypyrrole and those of Si-core staffanes similar to polysilanes, if one compares the values calculated with the same method.

Another observation is that electronic properties of large conjugated polymers are probably not optimally treated by present DFT methods and care should be taken when evaluating such results.

5. Heavy-Core Staffanes and Polaron Properties

There are only a few organic polymers that are semi-conducting or conducting in their neutral state; oxidation or reduction (p- or n-doping) is generally required. In this chapter the main features of the oxidized heavy-core staffanes will be discussed and compared to oxidized oligothiophene, oligosilane and oligostannane.

In solid-state physics, a *polaron* is a local distortion in the crystal structure creating a potential well where a charge, positive (hole) or negative (electron), becomes localized. In chemical terminology it is the equivalent of a geometrical distortion in a molecule that localizes a radical ion after oxidation or reduction, *Figure 21*.

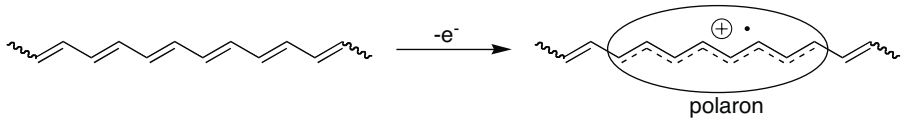

Figure 21. Localized polaron upon oxidation.

This localization is energetically favorable, which could sound counter-intuitive to what usually is thought of for electron delocalization in conjugated systems. In polyacethylene the energy gain of delocalizing the polaron over three -bonds instead of two is less than the energy gained by delocalization over two instead of one. After delocalizing the charge over a number of -bonds the energy gain from an additional -bond becomes smaller than the Jahn-Teller distortion energy, which is described in chapter 1.2. As a consequence, the polaron becomes geometrically constrained to a segment of the polymer, and the length of this segment differs from polymer to polymer.

5.1. Ionization Potentials

The energy required to remove or add an electron to a molecule can be calculated in different ways. The simplest is to use Koopmans' theorem, which states that the HF MO-energy from which the electron is abstracted (or added to) equals the negative of the ionization potential (IP) (or electron

affinity (EA)). This method is a rough approximation since electron correlation is not considered. A more rigorous, but much more computationally expensive way to obtain ionization potentials and electron affinities is through the ROVGF formalism, where the poles of a Green's function correspond to the IP's and EA's.[82] Yet another way to obtain the oxidation potential is to calculate the energy difference between E_0 and E_+^* in *Figure 22*, which can be done with any computational method (e.g. B3LYP and MS-CASPT2).

5.2. Internal Reorganization Energies

The internal reorganization energy λ_i is a measure of the activation energy needed to move a polaron from one segment of a polymeric chain to another in the solid state. A low reorganization energy gives a high charge mobility, as the polaron is less bound. If the polaron traps are degenerate and the temperature is high enough to allow vibrational modes to be treated classically, the standard formulation of Marcus/Hush for charge transfer rate k_{CT} is expressed as

$$k_{CT} = \sqrt{\frac{\pi}{\lambda k_b T}}\frac{1}{\hbar}V^2 \exp\left(-\frac{\lambda}{4k_b T}\right) \qquad (5.1).$$

At a given temperature T, the rate is dependent on the electronic coupling term V and the reorganization energy λ. For a system including solvent, λ can be separated into λ_i and λ_s (solvent reorganization energy). However, in a solid where there is no solvent present, only λ_i contributes which can in turn be defined by

$$\lambda_i = \lambda_0 + \lambda_+ = \left(E_0^* - E_0\right) + \left(E_+^* - E_+\right) \qquad (5.2).$$

Here the subscript "0" denotes the energy for the relaxation of the distorted ground state back to equilibrium geometry, subscript "+" the relaxation of the radical cation to equilibrium geometry and superscript "*" the vibrationally excited state, *Figure 22*. The method of calculating λ_i is through the energy differences given in (5.2), see also *Figure 22*.

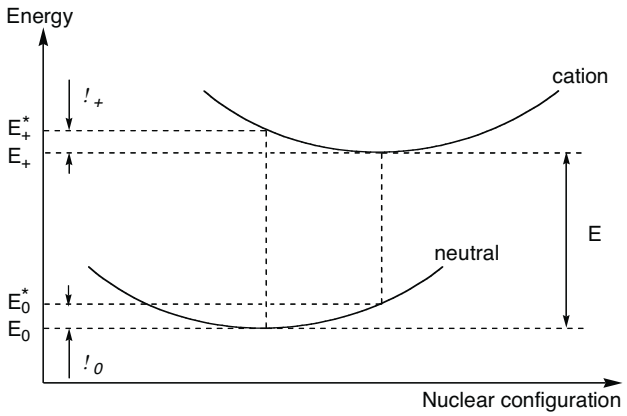

Figure 22. Definition of λ_0 and λ_+ for calculation of λ_i.

In the solid state of polymers the internal reorganization energy has been found to be the rate-limiting factor for charge transfer.[83] This opens up for a relatively easy computational first step in the design of novel oligo/polymeric compounds suitable for hole transport.

5.3. Spin and Charge Delocalization

To be able to assess the extent of the charge delocalization in the radical cations, the amounts of excess charge and spin per atom have to be estimated. As the charge of an atom in a molecule is not uniquely defined it has to the calculated according to a chosen model. In this thesis the *natural population analysis* (NPA) is used to estimate atomic charge.[84] The NPA method is more robust than the Mulliken analysis since it is less dependent on a well-balanced basis set.

5.4. Computational Results

5.4.1. Geometries of Neutral Staffanes

In the heavy-core staffane it is of interest to see how inter-cage bond distances and through-space distances change upon oxidation, and how variations in distances are distributed along the oligomer. Eight units long oligomers of all-C, Si- and Sn-core staffanes have been geometry optimized both in their ground and oxidized states to investigate this matter.

For optimized geometries in the neutral ground state of C-, Si- and Sn-core [8]staffanes at different levels of theory there are only small changes to notice. Using MP2/cc-pVDZ (for C) /LANL2DZp (for Si and Sn) as refer-

ence, the M···M through-space distances and M-M bonds length calculated with B3LYP and HF level differ by 0.03 Å at the most. B3LYP agrees well with MP2 for the M···M distances for C, Si and Sn. With regard to the M-M bond length, MP2 and RHF are most similar when M = Sn, but when M = C or Si RHF and B3LYP are more similar. As seen in Chapter 3, the through-space M···M distance in 1,3-disila/stannabicyclo[1.1.1]pentane is similar, or shorter than a normal Si-Si/Sn-Sn bond, while the C···C distance in 1,3-bicyclo[1.1.1]pentane is much longer than a regular C-C bond. This relation also holds for the corresponding staffanes, *Figure 23*.

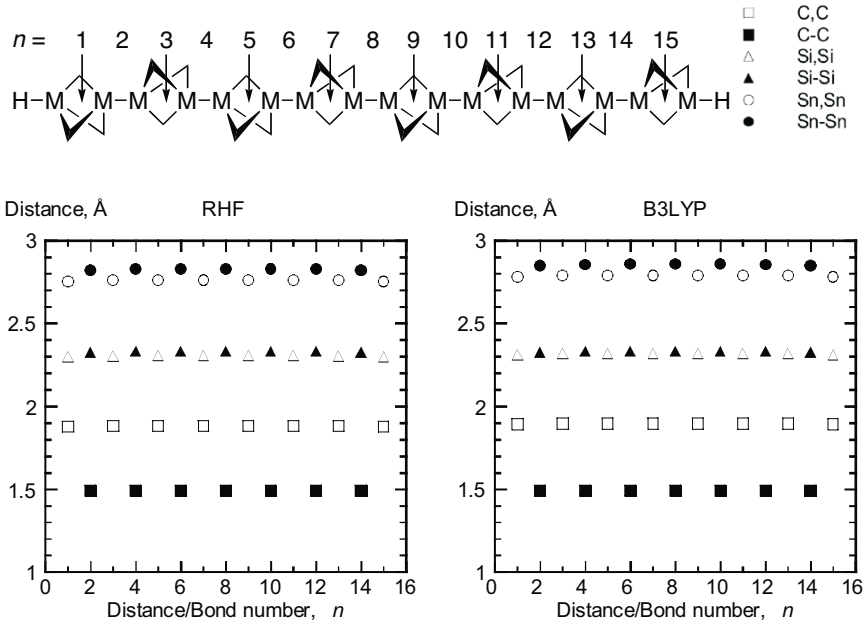

Figure 23. M-M bond lengths (filled symbols) and M···M through-space distances (empty symbols) for C-, Si- and Sn-core [8]staffanes in their neutral ground state, calculated at RHF level (left), B3LYP level (right), both with the basis set cc-pVDZ (for C) and LANL2DZp (for Si and Sn).

5.4.2. Geometries of Radical Cations

Upon oxidation, the geometry changes to best accommodate the polaron. Here the two methods, ROHF and B3LYP produce some different results when the change in bond length between the neutral and radical cationic state is calculated, *Figure 24*. When the all-C-[8]staffane is oxidized, ROHF produces large distortions at the central C-C bond, an elongation of 0.24 Å, while the through-space distances of the two central cages shorten by 0.14 Å, *Figure 24*. For Si and Sn at the bridgehead positions the elongation of the

central bond is smaller, and the shortening of the through-space distance is less compared to the C-staffane. The larger change in the central bond for the C-staffane should imply that this bond is weakened more than in the case of the Si and Sn-core staffanes, and that the polaron is localized in the all-C staffane.

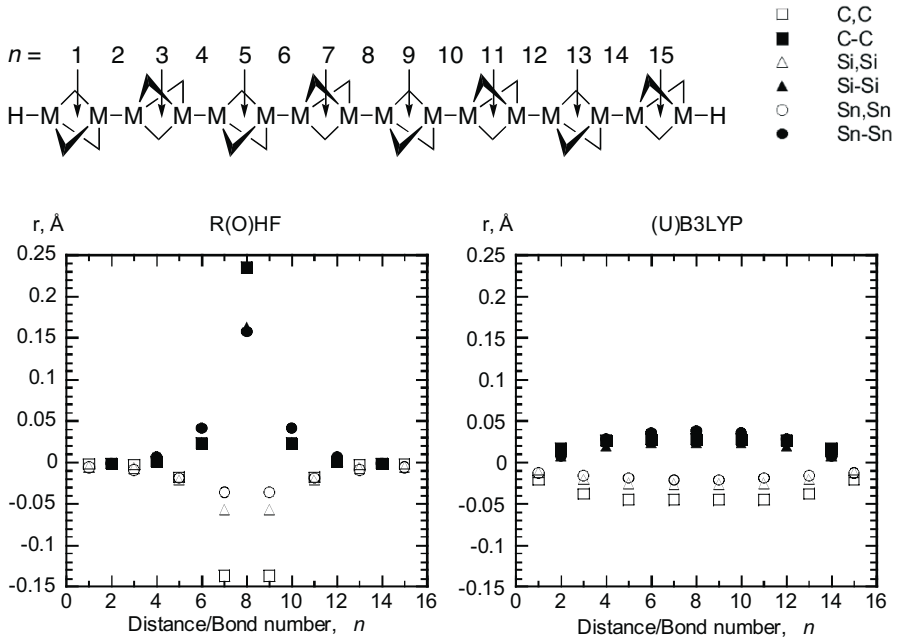

Figure 24. M···M distance and M-M bond length differences between neutral and radical cationic C-, Si- and Sn-core staffanes at R(O)HF (left) and (U)B3LYP (right) level, both with the basis set cc-pVDZ (for C) and LANL2DZp (for Si and Sn).

On the other hand, the B3LYP method distributes the geometry changes upon oxidation over essentially all M-M bonds and M···M distances. Consequently, the change per bond is smaller. Again, the C-staffane displays the largest change in the distance of the central bond of the staffanes. However, at this level of computation the bond is only elongated by 0.03 Å. The Si- and Sn-core staffanes display smaller changes for the central M-M bond when going from the neutral to oxidized state, *Figure 24*. With both HF and B3LYP the changes in the methylene bridge bonds are small for all the investigated [8]staffanes, less than 0.02 Å.

Both methods reveal that the geometric distortion upon oxidation is larger and more localized for the C-staffane than for the staffanes with heavier bridgehead elements. Previous studies on oligothiophene radical cations where results from HF and hybrid functional DFT calculations were compared against those from UMP2 calculations concluded that HF is better able

to describe the self-localization of a polaron than hybrid DFT methods.[85] However, hybrid functionals were believed to produce results that can be used semi-quantitatively as opposed to pure DFT functionals that completely fail to describe the self-localization of the polaron.

5.4.3. Ionization Potentials

Comparing the values of the ionization potentials (IP's) calculated at ROVGF/6-311G(d) and B3LYP/cc-pVDZ (for C) and LANL2DZp (for Si and Sn) it can be seen that there is an overall good agreement, Table 4, with slightly lower values obtained with the B3LYP method.

Extrapolation of the IP's from B3LYP using an inverse polynomial function to obtain an estimate of the IP in a polymer reveal that the polymeric Sn-core staffanes will have the lowest IP of the three investigated staffanes. The same method applied to permethylated polysilanes and polythiophenes give IP's at infinite length of 5.67 and 4.97 eV, respectively. Thus the permethylated polysilane and polymeric Si-core staffane will have the same IP.

Table 4. *Ionization potentials of M-core [n]staffanes calculated with ROVGF/6-311G(d) and B3LYP/cc-pVDZ (for C) /LANL2DZp (for Si and Sn), and with extrapolated infinite values at B3LYP level.*

M =	C		Si		Sn	
n	IP (eV) ROVGF	IP (eV) B3LYP	IP (eV) ROVGF	IP (eV) B3LYP	IP (eV) ROVGF	IP (eV) B3LYP
1	10.65	10.62	9.93	9.46	8.39	8.43
2	9.51	9.39	8.30	8.23	7.65	7.71
3	9.03	8.83	7.65	7.54	7.04	7.05
4	8.78	8.50	7.33	7.12	6.73	6.68
5		8.28		6.91		6.45
8		7.93		6.51		6.10
12		7.63		6.25		5.86
16		7.48		6.08		5.74
20		7.37		6.02		5.66
∞		6.97		5.67		5.36

5.4.4. Internal Reorganization Energies

The calculations of the internal reorganization energies, $_i$, were performed at (U)B3LYP and (U)MP2 level using cc-pVDZ (for C) and LANL2DZp (for Si and Sn), Table 5. From the results it is evident that the staffanes with heavier M atom at bridgehead positions require less energy for the geometrical displacement of a polaron. These results should be compared to that of

oligothiophene with 20 monomer units, which has a $_i$ of 0.083 eV at the B3LYP level of theory.

Table 5. *Calculated internal reorganization energies for M-core [n]staffanes calculated at (U)B3LYP (normal print) and spin projected (U)MP2 (italics) levels using the cc-pVDZ for C- and LANL2DZp for Si- and Sn-core staffanes. Values in eV.*

n	M = C	M = Si	M = Sn	[n]thiophenes
2	1.472, *1.496*	0.356, *0.402*	0.252, *0.309*	0.345
3	1.093 *1.127*	0.281, *0.322*	0.184, *0.212*	0.306
4	0.877, *0.942*	0.232, *0.266*	0.144, *0.180*	0.274
5	0.716, *0.896*	0.201, *0.249*	0.121, *0.160*	0.237
8	0.478	0.126	0.095	0.208
12	0.294	0.081	0.054	0.146
16	0.223	0.062		0.106
20	0.176	0.047		0.083

The short staffanes and oligothiophenes were calculated with (U)MP2 to investigate the agreement with the B3LYP results. It was found that (U)MP2 in general gives 20% higher $_i$ compared to B3LYP. However, due to significant spin contamination of the UHF wavefunction for longer radical cationic M-staffanes, the longest oligomer calculated at (U)MP2 level is that with five monomers. For oligothiophenes very high spin contamination was also found in shorter oligomers and the $_i$ are therefore not given here.

5.4.5. Charge and Spin Delocalization

The charge and spin distribution in C-, Si- and Sn-core staffanes were calculated using the RHF and B3LYP methods, as in Chapter 5.4.2. Considering the differences between the two methods for estimating bond length differences, a coherent behavior was not to be expected for charge and spin localization. The calculated charge localizations in the radical cations of C-, Si and Sn-core staffanes are plotted in *Figure 25.* At the ROHF level, the spin density distributions for the [8]staffane radical cations essentially agree with the corresponding charge distributions with localization at the two central M-atoms. At the (U)B3LYP level a more delocalized polaron is calculated, *Figure 25*.

Consequently, the same trend is seen for the charge and spin density distributions as for the bond length differences. The ROHF method gives a higher localization of the polaron in the middle of the oligomer, and this localization is slightly attenuated when M = Si or Sn. At the (U)B3LYP level the charge and spin is more delocalized, and now the trends between the these different M-core staffanes is absent as the distributions are essentially equal.

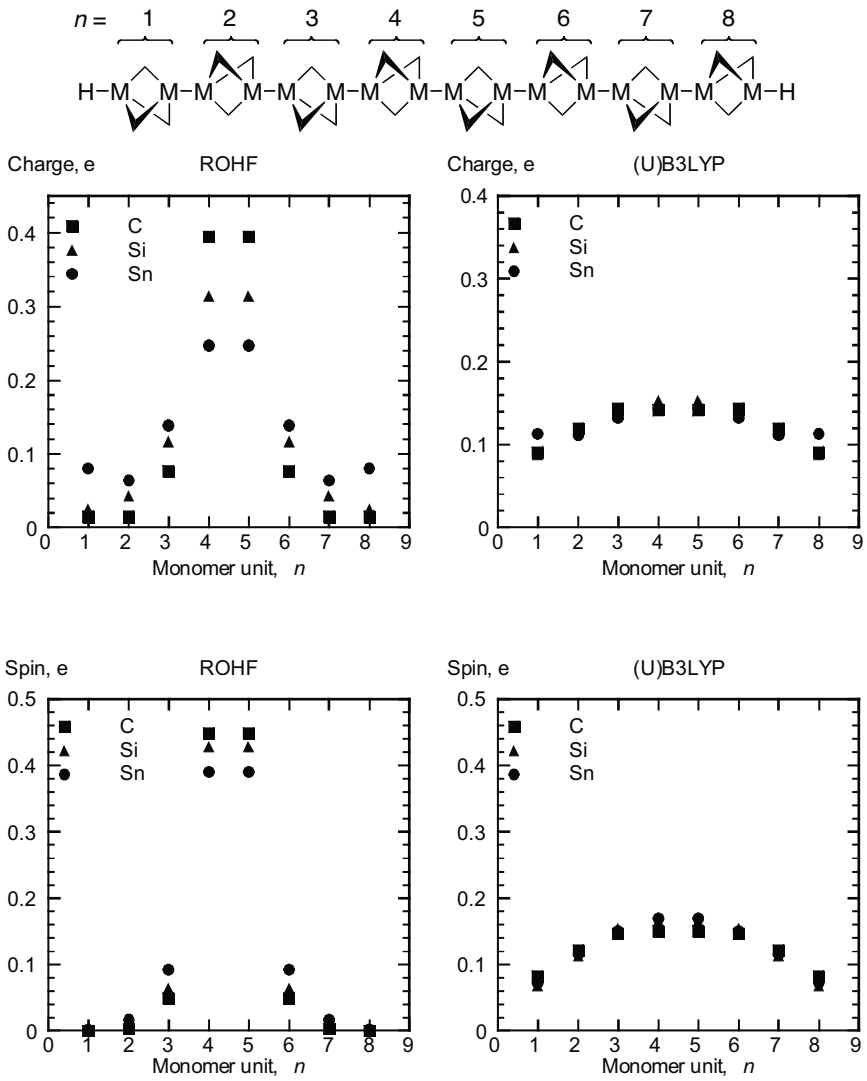

Figure 25. Top: Charge per monomer unit in the radical cations of C-, Si- and Sn-core [8]staffanes. Bottom: Spin delocalization in the radical cations of C-, Si- and Sn-core staffanes, calculated at ROHF (left) and (U)B3LYP (right) using cc-pVDZ for C-core and LANL2DZp for Si- and Sn-core staffanes.

5.5. Synopsis

The calculations of the Si- and Sn-core staffanes show that these molecular wires should have ionization potentials in the same range as polysilanes, and internal reorganization energies similar to those of polythiophenes.

When assessing the extent of the polaron localization along an oligomer chain, the choice of computational method plays an important role. Previous studies have concluded that RHF has an advantage over pure DFT methods, and also to some extent over hybrid DFT functionals.[85] This is also seen in this study where charge, spin and bond length differences between neutral and radical cation oligomers were computed. However, the overall picture of the extent of the polaron localization is that it is more localized in the C-core staffane as compared to the Si and Sn-core staffanes.

6. Excited Electronic States of Small Silicon Containing Bicyclic Compounds

To be able to probe the spectroscopic properties of two Si-Si bonds separated spatially by a cage structure, this investigation focused on the valence excitation energies of two molecules with close resemblance to 1,3-disilabicyclo[1.1.1]pentane (**1b**). The reason for not investigating **1b** is because its high symmetry, D_{3h}, makes the type of calculations that are needed more complex and erroneous results can be obtained. Instead, two compounds with close resemblance to **1b**, 1,4-disilabicyclo[2.2.1]heptane (**21**) and 1,4-disilabicyclo[2.1.1]hexane (**22**), both with silyl- or trimethylsilyl- (TMS) groups attached to the Si bridgehead atoms, were investigated, *Figure 26*.

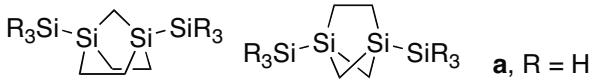

21 **22**

Figure 26. 1,4-Disilabicyclo[2.2.1]heptane **21** and 1,4-disilabicyclo[2.1.1]hexane **22**.

With these molecules one can study both the effect of cage size as well as the effect of the substituent (H or Me) on the terminal silicon atoms on the excitation properties.

6.1. Vertical Excitation Energies and Oscillator Strengths

When a molecule interacts with an external electromagnetic field with proper frequency, it can absorb energy and become promoted to an excited state, *Figure 27*. The excited state can be an electronically, vibrationally, or rotationally excited state. In this thesis, vertical electronic excitation energies have been investigated, i.e. excitations for which the nuclear configuration does not change from the equilibrium ground state geometry. This is a rea-

sonable assumption as the change in electronic state occurs on a much shorter time scale than the motion of the nuclei.

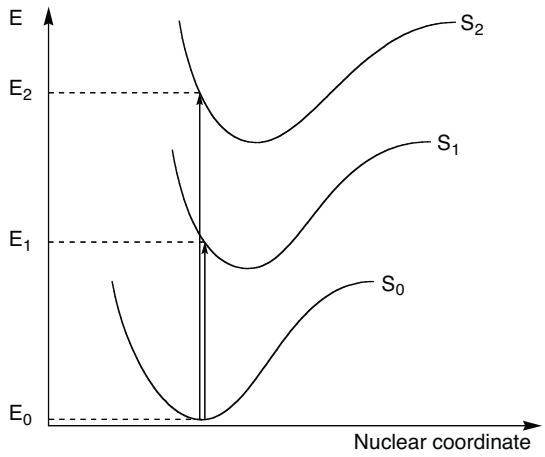

Figure 27 Schematic drawing of vertical excitations, S_0 is the electronic ground state, S_1 the first electronically excited state and S_2 the second electronically excited state. E_1 and E_2 are the vertical excitation energies.

Whether the optical transition between two electronic states is physically allowed or not is given by the selection rule,

$$\Gamma_{GS} \otimes \Gamma_{p} \otimes \Gamma_{XS} \supset \Gamma_{Sym} \qquad (6.1).$$

For the transition to be allowed, the product of the irreducible representation of the ground state Γ_{GS}, excited state Γ_{XS}, and the dipole operator Γ_{p}, should belong to the totally symmetric irreducible representation Γ_{Sym}. The irreducible representations of dipole operator and the totally symmetric operator are given in the character tables for any given symmetry point group.[86]

The excitation energies presented in this thesis are calculated as the difference in energy between the ground state and the excited state. To compute the energies of the different states with a high accuracy, the CASPT2 and MS-CASPT2 methods were used.

The intensity of a dipole allowed transition is given by the oscillator strength *f*. It can be calculated in different ways, and the one used for the results in this chapter is

$$f = \frac{2}{3}\left(\mathrm{TDM}\right)^2 \ \mathrm{E} \qquad (6.2),$$

where TDM is the transition dipole moment and E the energy difference between the two electronic states between which the electronic transition takes place. The transition dipole moment is computed with the CASSCF state interaction method using the PMCAS wavefunction and the energies from the MS-CASPT2 calculation.[87,88]

The focus of this investigation has been on excitations to states in which the valence electrons are excited to unoccupied MO-type valence orbitals. However, there can also be Rydberg states in the same energy region of the spectrum. These states have very diffuse spatial distributions since the excitation to Rydberg states lifts the electron(s) into orbitals that have the appearance of large atomic orbitals with the molecule at the charge center.

When calculating excited states in a region where both valence and Rydberg states can be present, it is desirable to avoid their mixing since the computed results are then likely to be misleading. This can be handled in different ways. If the molecule is small or the method is computationally less demanding, a basis set with a set of properly designed Rydberg-type basis functions can be used to describe to Rydberg states explicitly. For more computationally demanding methods where the number of orbitals that can be useed is limited, e.g. CASPT2, different techniques have to be applied. The MS-CASPT2 method has shown to reduce the problem of strong mixing of valence and Rydberg states in the CASPT2 calculation, which can be introduced by the preceding CASSCF calculation. This mixing is due to insufficient number of virtual orbitals included in the active space, giving rise to so-called intruder states in the CASPT2 calculation. In the calculations presented in this work, where intruder state interactions were detected they were dealt with by careful selection of the active space in the CASSCF calculation, the multistate technique, proper number of calculated excited states and by the level shifting technique.[89]

TD-DFT calculations

In addition to the MS-CASPT2 technique other methods for calculation of excitation energies were also attempted, mainly *time-dependent* DFT (TD-DFT). Although a large number of different functionals and basis set combinations were tested no systematic improvement with increasing level of theory was observed. For some combinations reasonable excitation energies, when compared to MS-CASPT2 values, could be obtained. However, the relative oscillator strengths for the lowest transitions were always far from agreement with the MS-CASPT2 values.

6.2. Results

6.2.1. Geometries

Geometry optimizations were first performed at B3LYP/6-31G(d) level and confirmed as minima by frequency calculations. The symmetry of the ground state is C_{2v} for all four molecules. The stationary points were then further optimized at MP2/cc-pVTZ level and the resulting geometries were used for the excited state calculations.

The coordinate system is chosen so that the principal C_2 rotational axis is parallel to the z-axis, *Figure 28*. For **21a** the yz-plane is set to include the four Si-atoms and the methylene bridge carbon, and for **22b** the four Si-atoms and the ethylene bridge carbons are in the yz-plane. In this study the yz-plane is set as the plane that defines the MO's as being of ! - or -type.

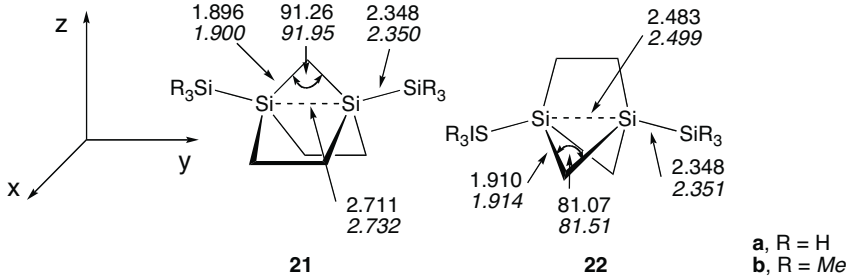

Figure 28. Geometrical features of **21a**/**21b** and **22a**/**22b** at MP2/cc-pVTZ level, with **21a** and **22a** in normal print and **21b** and **22b** in italics. Bond lengths in Å and angles in deg. The coordinate system defines the symmetry elements with z as the principal rotational axis.

The through-space Si···Si distances in **21** are 2.71 Å (**21a**) and 2.73 Å (**21b**), respectively, whereas in **22** these distances are more than 0.2 Å shorter, *Figure 28*. This is the main difference in geometrical features between the two sets of molecules. Thus, the through-space distances are longer than a normal Si-Si single bond by 0.35 and 0.15 Å. This can be compared to **1b** (Chapter 3) where the through-space distance is only 2.30 Å. Other geometrical differences are small when changing an ethylene bridge to a methylene bridge and/or substituents on the terminal silicon atoms.

6.2.2. Ionization Potentials

The ionization potentials were calculated at MS-CASPT2 and ROVGF/6-311G(d) level on geometries optimized at MP2/cc-pVTZ level. The results are listed by electronic state in Table 6 for **21** and Table 7 for **22**.

Generally, the values obtained at the ROVGF level agree with the vertical ionization potential values at the MS-CASPT2 level, with two excep-

tions. For **22a** and **22b** the ionization of the 2^2B_2 state are ~0.3 eV lower with the MS-CASPT2 method, indicating a small mixing of the two highest occupied b_2 orbitals in those molecules. This is properly handled by the multireferent CASSCF technique in the MS-CASPT2 method, in contrast to the ROVGF method where only dynamic electron correlation is taken into account.

Table 6. *Calculated Ionization Potentials in eV at MS-CASPT2 and ROVGF level of theory of **21a** and **21b**.*

	21a		**21b**	
state	MS-CASPT2	ROVGF[a]	MS-CASPT2	ROVGF[a]
1^2B_2	8.80	8.82 (9.83) [b]	7.81	7.91 (9.06) [b]
2^2B_2	9.31	9.35 (10.55)	8.83	8.91 (10.16)
1^2A_2	8.75	8.84 (10.05)	8.32	8.43 (9.68)
1^2A_1	9.41	9.66 (10.73)	8.56	8.79 (9.97)
1^2B_1	10.76	10.79 (12.15)	9.93	10.19 (11.54)

[a] Calculated at ROVGF/6-311G(d)//MP2/cc-pVTZ level.
[b] Ionization potential according to Koopmans' theorem at HF/6-311G(d)//MP2/cc-pVTZ level.

Table 7. *Calculated Ionization Potentials in eV at MS-CASPT2 and ROVGF level of theory of **22a** and **22b**.*

	22a		**22b**	
state	MS-CASPT2	ROVGF[a]	MS-CASPT2	ROVGF[a]
1^2B_2	8.42	8.45 (9.40) [b]	7.48	7.57 (8.65) [b]
2^2B_2	8.88	9.15 (10.28)	8.34	8.66 (9.85)
1^2A_2	9.27	9.35 (10.42)	8.82	8.92 (10.05)
1^2A_1	9.70	10.04 (11.15)	8.88	9.21 (10.41)
1^2B_1	10.42	10.49 (11.87)	9.95	10.02 (11.42)

[a] Calculated at ROVGF/6-311G(d)//MP2/cc-pVTZ level.
[b] Ionization potential according to Koopmans' theorem at HF/6-311G(d)//MP2/cc-pVTZ level.

The reductions in the IP when substituting hydrogen with methyl at Si are likely to be a substituent inductive effect since the first IP corresponds to the removal of an electron from the $_{SiSi}$ (HOMO) in agreement with observations for other disilanes.[90] More interesting is the decrease in the first IP when changing the cage size, i.e. when going from **21a** to **22a**, and from **21b** to **22b**. This would reflect the extent of the interaction between the two Si-Si bonds, as the decrease is 0.38 and 0.33 eV (at MS-CASPT2 level) for **21a**/**22a** and **21b**/**22b**, respectively. As the two compound types only differ by a CH_2 unit, the lowering is likely to stem from the decrease in Si···Si through-space distance by 0.2 Å. If the two bonds where non-interacting, one could also reason that the first IP should have closer resemblance to Si_2Me_6 (8.7 eV),[91] however, their IP's are lower by 0.9 and 1.2 eV, respec-

tively. The value calculated for the first IP's of **21b** and **22b** are even lower than the value obtained for $Si_2(t\text{-}Bu)_6$ (8.1 eV) which has a very extended Si-Si bond of 2.69 Å.[92]

6.2.3. Electronic Excitations

Computational Details

Benchmarking was performed in order to ensure that the proper parameters were used in the MS-CASPT2 calculations. Since all four molecules are calculated with C_{2v} symmetry, electrons and orbitals have to be properly chosen among the four irreducible representations a_1, b_2, a_2 and b_1. It was concluded that to satisfactory describe the valence excited states, the CASSCF calculation needed 10 electrons together with an active space constructed from 12 orbitals. In the ground state, the occupied orbitals in the active space consist of one a_1, two b_2, one a_2 and one b_1 symmetric orbital. The number of virtual orbitals needed was three a_1, two b_2, one a_2 and one b_1 symmetric orbital. The same combination was found to be required for all four compounds. The orbitals in the active space of **21a** and **22a** are seen in *Figure 29* and *Figure 30*, respectively. The orbitals in the active spaces of **21b** and **22b** have close resemblance to the orbitals shown in *Figure 29* and *Figure 30*, with the addition of some contribution at the methylated terminal silicon atoms.

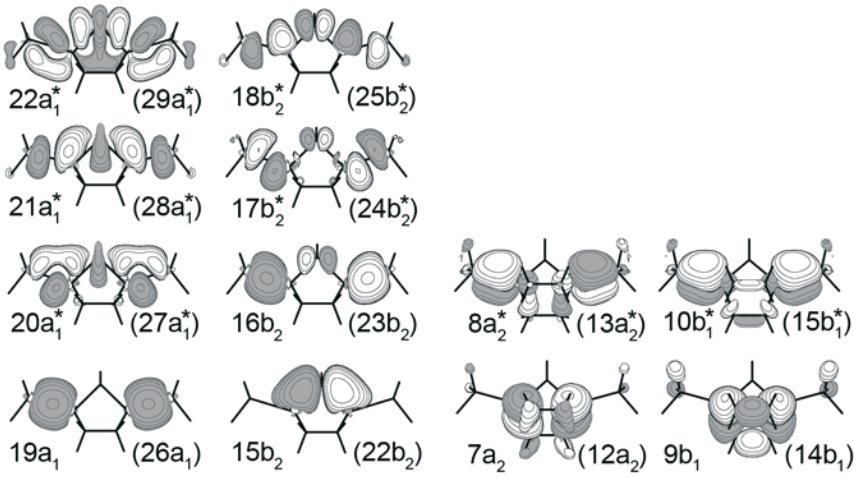

Figure 29. Plot of state-average orbitals of the active space for the ground state of **21a**, labeled by symmetry and number. Numbers marked with "*" indicate unoccupied orbitals in the ground state. Labels in parenthesis refer to the corresponding orbitals for **21b**.

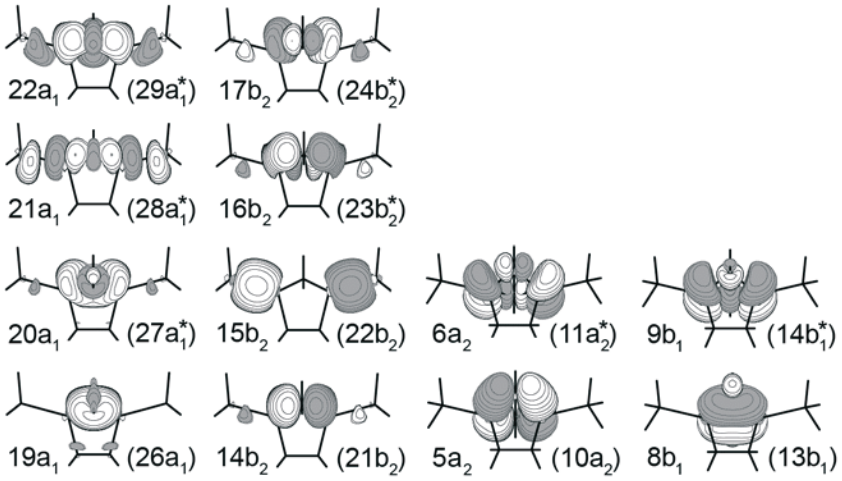

Figure 30. Plot of state-average orbitals of the active space for the ground state of **22a**, labeled by symmetry and number. Numbers marked with "*" indicate unoccupied orbitals in the ground state. Labels in parenthesis refer to the corresponding orbitals for **22b**.

The labeling of the unoccupied orbitals and ordering them according the energy is not possible since orbitals within the active space do not have energies. This also applies to the occupied orbitals within the active space, but by visual inspection and by comparing them to HF-orbitals one can assign them in HF-energy order. This is more difficult to do with the unoccupied orbitals, since they in several cases for these molecules do not have clear resemblance to the unoccupied HF orbitals. Therefore the active space orbitals will be assigned by MO-symmetry type as a_1, b_2, a_2 and b_1, plus the number of the respective order within each symmetry type. The numbering of the active space orbitals is shown in *Figure 29* and *Figure 30*, for **21a**,**b** and **22a**,**b** respectively.

For the occupied orbitals of **21a** and **21b**, the a_1 orbital and one b_2 orbital correspond to the Si-Si bond, one b_2 orbital correspond to the methylene bridge bonds and the a_2 and b_1 orbitals to the ethylene bridge bonds. Of the virtual orbitals in **21a** and **21b**, the three a_1 symmetric orbitals correspond to the Si-Si bonds, the Si-methylene bridges and to the Si-H or Si-C bonds of the end groups. The virtual b_2 orbitals correspond to the Si-Si bonds and the Si-methylene bridges, while the a_2 and b_1 orbitals correspond to Si-Si bonds.

In **22a** and **22b**, the a_1, a_2, b_1 and one b_2 occupied orbitals correspond to the bonds in the methylene bridges, and one b_2 orbital corresponds to the Si-Si bonds. For the virtual orbitals one a_1 and one b_2 orbital describe the Si-Si bonds, one a_1 and one b_2 orbital the out-of-plane Si-methylene bonds, and one a_1 orbital the C-H bonds of the methylene bridges. The a_2 and b_1 virtual

orbitals correspond to the cage Si atoms and their interaction with the methylene bridges.

Results

With regard to the nature of the excited states for all four molecules they are, with few exceptions, all of multireferent character and thus difficult to describe in pictures because the occupation numbers of the corresponding natural orbitals are not close enough to singly or doubly occupied. Instead the analysis of the composition of the excited states is given in the weight (%) of CASSCF configurations in the final wavefunction for a given state, see Table 8.

Table 8. *MS-CASPT2 vertical excitation energies (eV), oscillator strengths as well as main configurations (>20%) and weights (%) of **21a** and **21b**.*

21a				**21b**			
State	Energy	*f*	W(%), configuration	State	Energy	*f*	W(%), configuration
1^1B_2	6.00	0.39	50% $16b_2$ $20a_1$*	1^1B_2	5.51	0.35	58% $23b_2$ $27a_1$*
			34% $15b_2$ $20a_1$*				21% $23b_2$ $29a_1$*
1^1A_2	6.01	0	86% $7a_2$ $20a_1$*	1^1A_2	5.78	0	69% $12a_2$ $27a_1$*
							25% $12a_2$ $28a_1$*
2^1A_1	6.20	0.08	90% $7a_2$ $8a_2$*	2^1B_2	5.92	0.10	48% $23b_2$ $28a_1$*
							29% $22b_2$ $28a_1$*
2^1A_2	6.24	0	58% $7a_2$ $21a_1$*	2^1A_2	5.95	0	41% $12a_2$ $28a_1$*
			34% $7a_2$ $22a_1$*				38% $12a_2$ $27a_1$*
1^1B_1	6.39	0.08	73% $7a_2$ $17b_2$*	2^1A_1	5.97	0.06	79% $23b_2$ $24b_2$*
2^1B_2	6.45	0.15	50% $16b_2$ $20a_1$*	3^1B_2	6.07	0.02	84% $12a_2$ $15b_1$*
			34% $15b_2$ $20a_1$*				
3^1A_1	6.50	0.18	36% $16b_2$ $17b_2$*	1^1B_1	6.09	0.11	47% $23b_2$ $13a_2$*
			22% $16b_2$ $18b_2$*				40% $22b_2$ $13a_2$*
3^1B_2	6.58	0.07	52% $16b_2$ $21a_1$*	3^1A_2	6.09	0	57% $23b_2$ $15b_1$*
							23% $22b_2$ $15b_1$*
2^1B_1	6.61	0.13	54% $16b_2$ $8a_2$*	3^1A_1	6.19	0.12	45% $26a_1$ $27a_1$*
			35% $15b_2$ $8a_2$*				33% $22b_2$ $25b_2$*
3^1A_2	6.75	0	48% $16b_2$ $10b_1$*	2^1B_1	6.27	0.01	79% $12a_2$ $24b_2$*
			39% $19a_1$ $8a_2$*				
4^1B_2	6.99	0.06	54% $15b_2$ $22a_1$*	4^1B_2	6.33	0.19	63% $22b_2$ $27a_1$*
			23% $16b_2$ $21a_1$*				23% $23b_2$ $29a_1$*

With regard to the oscillator strength of the transitions it should be noted that the dipole transition operator in C_{2v} symmetric systems is $(A_1+B_1+B_2)$, [†] which effectively makes only the A_2 transitions symmetrically forbidden.

21a** and **21b: To avoid the most troublesome energy regions where Rydberg states are present, only electronic states with energies 1.5 - 2 eV below the first ionization potential, as approximated by MS-CASPT2 calculations, were considered. This is based on previous experience with similar calcula-

[†] See Appendix

tions on small silicon oligomers. For **21a** this limit is around 7.0 eV and for **21b** it is at 6.3 eV. States with energies below these values are listed in Table 8 in order of energy, together with the CASSCF configurations and their weights.

The dipole allowed vertical transitions that have significant intensity for **21a** are located in two intervals of the spectrum. The strongest transition (0.39) of #-#* character, is to the 1^1B_2 state at an energy of 6.0 eV, and is almost degenerate with the transition to the 1^1A_2 state at 6.01 eV (-#*). The second band is centered at 6.5 eV and is composed of transitions to the 1^1B_1 (!#*), 2^1B_2 (#-#*), 3^1A_1 (#-#*), 3^1B_2 (#-#*) and 2^1B_1 (#- *) states. The 2^1B_2, 3^1A_1, and 2^1B_1 transitions are the strongest contributors to this band, with oscillator strengths of 0.15, 0.18 and 0.13 respectively.

Replacing the H atoms of the silyl groups by methyl groups (**21b**) results in a spectrum with two intervals with strong oscillator strengths. The first centered around 5.5 eV, mainly composed of the transition to the 1^1B_2 state (#-#*), and the second band around 6.2 eV is made up from the 2^1B_2 (#-#*), 1^1B_1 (#- *), 3^1A_1 (#-#*) and 4^1B_2 (#-#*) transitions, where the latter transition is the strongest contributor (0.19).

22a** and **22b: For **22a**, the first ionization potential is 8.4 eV according to MS-CASPT2 calculations, and for **22b** it is 7.5 eV. In Table 9 we therefore list excitations up to 6.9 and 6.1 eV, respectively, together with the CASSCF configurations and their weights.

In **22a** the two lowest transitions are to dark states of A_2 symmetry at 5.10 and 5.74 eV and which both are of #! * character. The lowest allowed transition is into the 1^1B_2 state (#-#*) at 5.81 eV, which also is the strongest transition (0.77). Together with the transitions to the 2^1B_2 (#-#*) and 2^1A_1 (#-#*) states it makes up the first band in the spectrum of **22a**. A second band arises from the transition to the 3^1A_1 state (#-#*) at 6.41 eV. In **22b** the lowest transition is to the 1^1A_2 at 4.76 eV. The transitions with strong or moderate oscillator strengths are to the 1^1B_2 state (#-#*) at 5.37 eV, to the 2^1B_2 state (- *) at 5.68 eV, the strongest in the spectrum, and to the 1^1B_1 state (#- *) at 6.01 eV.

Table 9. *MS-CASPT2 vertical excitation energies (eV), oscillator strengths as well as main configurations (>20%) and weights (%) of **22a** and **22b**.*

22a				**22b**			
State	Energy	*f*	W(%), configuration	State	Energy	*f*	W(%), configuration
1^1A_2	5.10	0	75% $15b_2$! $9b_1$*	1^1A_2	4.76	0	64% $22b_2$! $14b_1$*
							27% $21b_2$! $14b_1$*
2^1A_2	5.74	0	76% $14b_2$! $9b_1$*	1^1B_2	5.37	0.25	48% $22b_2$! $27a_1$*
							30% $21b_2$! $27a_1$*
1^1B_2	5.81	0.77	60% $15b_2$! $20a_1$*	2^1A_1	5.56	0.05	71% $22b_2$! $23b_2$*
2^1B_2	6.00	0.16	75% $5a_2$! $9b_1$*	2^1A_2	5.68	0	64% $21b_2$! $14b_1$*
							27% $22b_2$! $14b_1$*
2^1A_1	6.13	0.07	78% $15b_2$! $16b_2$*	2^1B_2	5.69	0.45	81% $10a_2$! $14b_1$*
3^1B_2	6.23	0.01	61% $15b_2$! $21a_1$*	3^1B_2	5.74	0.03	43% $22b_2$! $28a_1$*
							23% $22b_2$! $29a_1$*
4^1B_2	6.38	0.03	86% $14b_2$! $20a_1$*	1^1B_1	6.01	0.15	80% $26a_1$! $14b_1$*
3^1A_1	6.41	0.12	80% $14b_2$! $16b_2$*	3^1A_1	6.08	0.03	69% $22b_2$! $24b_2$*
1^1B_1	6.88	0.08	65% $5a_2$! $16b_2$*	4^1B_2	6.11	0.02	49% $21b_2$! $27a_1$*
			30% $5a_2$! $17b_2$*				28% $22b_2$! $27a_1$*

Discussion

Both **21a** and **21b** have the lowest transition to the 1^1B_2 state, and this transition also has the strongest oscillator strength. The transition of the methyl substituted compound, **21b**, is red-shifted by 0.5 eV when compared to the hydrogen substituted one, **21a**. This transition is of #-#* character and the major contribution is from an excitation from the HOMO. For **21a** the near degeneracy of the 1^1B_2 and the 1^1A_2 states at 6.0 eV correlates with the very small difference in energy seen in the ionization potentials for this system, Table 6. This is not the case in **21b** where the hydrogens on the terminal Si atoms are substituted with methyl groups. Now the 1^1B_2 state is separated from the 1^1A_2 state by 0.3 eV, although the transitions are of the same character as in **21a**, #-#* type and -#* type, respectively. With regard to the transitions with medium oscillator strengths, they all have contributions from excitations out of the HOMO; the 2^1B_2, 3^1A_1, and 2^1B_1 states in **21a**, and the 2^1B_2, 1^1B_1, and 4^1B_2 states in **21b**. The change from hydrogen to methyl substituents at the terminal Si atoms red-shifts the excitations of **21** with an average of 0.42 eV with the exception of excitations where the high energy $7a_2$ orbital in **21a** have a large influence, in which case the red-shift is decreased by up to 0.2 eV.

Changing the H atoms on the terminal Si atoms to methyl groups in systems **22**, i.e. going from **22a** to **22b**, one can note an overall larger similarity of the transitions between these two systems than for molecules **21a** and

21b. Both **22a** and **22b** have the lowest allowed transition to the 1^1B_2 state, and this transition has the strongest oscillator strength for **22a** and the second strongest for **22b**. The 1^1B_2 transition of the methyl substituted compound is red-shifted by 0.5 eV compared to the hydrogen substituted one. This transition is of *%%** character and the major contribution is from the excitation out of HOMO. The transitions to the 2^1B_2 states, on the other hand are in both compounds of - * type and these excitations show medium and strong oscillator strengths, for **22a** and **22b** respectively. With regard to the forbidden excitations to the A_2 states, which are the two lowest transitions in **22a**, and the first and fourth transitions in **22b**, they are both from the HOMO. Furthermore, the red-shift upon methyl substitution at the terminal Si atoms of **22** is similar to that found for systems **21**, with an average 0.41 eV with a few exceptions. With regard to oscillator strength, the compound with methylated terminal Si atoms (**22b**) favor excitations with ! * character over excitations of *%% ** character when compared to **22a**.

A general trend is that the change from H atoms to methyl substituents at the terminal silicon atoms red-shifts the excitation with around 0.5 eV in compounds **21** and slightly smaller red-shift, around 0.4 eV, for compounds **22**, with a few exceptions.

More interestingly, when comparing 1,4-disilylsubstituted and 1,4-disilabicycloalkanes of the type **21** and **22** the lowest excitation regardless of symmetry is 0.8 to 0.9 eV red-shifted in the latter compound. If one compares the lowest dipole allowed transition the difference is smaller, only 0.1 to 0.2 eV. This can be rationalized by considering that in **21** the methylene bridge is in the symmetry plane including the long axis of the molecule, yz-plane in *Figure 28*. That is, along the conjugation axis of the molecule. In **22** the methylene bridges are out-of-plane and when exciting an electron from b_2 symmetric HOMO the lowest lying orbital, of b_1 symmetry *Figure 30*, the state is then of A_2 symmetry, i.e. the transition is symmetry forbidden.

If one compares the calculated result for **21b** and **22b** with the experimental results of hexamethyl and hexaethyl substituted disilanes one can see that they have similar excitation properties since the first 1^1B_2 excitation of **21b** and **22b** have some influence of *%# ** Si-Si bond orbital type, although the multiconfigurational character makes such a assignment less precise. The excitation to the 1^1B_2 states are with high intensity, and these excitations are at lower energies, 5.5 and 5.4 eV, for **21b** and **22b** respectively, when compared to hexaethyldisilane where the Si-Si bond *%# ** excitation is at 6.3 eV.[91]

6.3. Synopsis

The lowest excited state is not of the same character as in oligosilanes due to the bicycloalkane cage structure separating the Si-Si bonds, instead it is

rather similar to that of disilane. As the cage introduces an interaction between the two Si-Si bonds, there is a red-shift in the lowest valence excitations and the first IP. The red-shift compared to Si_2Me_6 is larger for the smallest cage, 1,4-disilabicyclo[2.1.1]hexane having the shortest through-space Si···Si distance. Also, the lowest valence excited states of **21** and **22** are red-shifted by the methyl groups on the terminal silicon atoms.

The placements of the shorter methylene bridges relative to the symmetry plane have large influence on the low energy part of the excitation spectra, as the out-of-plane methylene bridges give rise to dark low energy states. Also, replacing the methylene bridge by a silylene bridge will increase the through-bridge contribution and may be one way to further increase the interaction between the two Si-Si bonds.

7. Concluding Remarks

To summarize it can be concluded that neither of the heavy 1,(*n*+2)-dimetallabicyclo[*n.n.n*]alkanes, with *n* = 1, 2 or 3, are excessively strained, and that 1,3-dimetallabicyclo[1.1.1]pentane are even less strained than the bicyclo[1.1.1]pentane that has already been synthesized. From the perspective of ring strain, the 1,(*n*+2)-dimetallabicyclo[*n.n.n*]alkanes are realistic synthetic targets, even though the 1,3-dimetallabicyclo[1.1.1]pentanes become gradually more prone to hydrolysis with a heavy Group 14 element in 1- and 3-positions.

From the calculated results of the properties of oligomers of the 1,3-dimetallabicyclo[1.1.1]pentane, heavy-core staffanes, the conclusion can be made that heavier Group 14 elements at the bridgehead positions increase the polarizability, increase the conjugation, and reduce the band gaps. The values for the Sn-core staffanes are in the same range as those of polypyrrole and those of Si-core staffanes are similar to those of polysilanes, if one compares the values calculated with the same method.

The calculations of ionization potentials for Si- and Sn-core staffanes show that the computed values are in the same range as for polysilanes and their internal reorganization energies as those of polythiophenes. With regard to the extent of polaron localization, the overall picture is that it is more localized in the C-core staffane than in the Si and Sn-core staffanes. Although the result is sensitive to the choice of method, and care should be taken when assessing results obtained, especially when using DFT methods.

High level calculations of the valence excited state 1,4-disilyl- and 1,4-bis(trimethylsilyl)bicyclo[2.2.1]heptane and 1,4-disilyl- and 1,4-bis(trimethylsilyl)bicyclo[2.1.1]hexane were successfully carried out. The results concluded that although the bicyclic cage separates the two disilane chromophores, there is a red-shift of the lowest valence excitations in the [2.1.1] compounds compared to the [2.2.1] compounds. This is a consequence of the shorter through-space distance and shorter bridges and so allowing the two Si-Si bonds to interact more in the [2.1.1] bicyclic compounds.

Appendix: Conversion Factors and Symmetry Table

Table 10. *Conversion table for energy units.*

1 unit =	**hartree**	**kJ mol^{-1}**	**kcal mol^{-1}**	**eV**	**cm^{-1}**
hartree	1	2625.50	627.51	27.212	2.1947x10^{5}
kJ mol^{-1}	3.8088x10^{-4}	1	0.23901	1.0364x10^{-2}	83.593
kcal mol^{-1}	1.5936x10^{-3}	4.1840	1	4.3363x10^{-2}	349.75
eV	3.6749x10^{-2}	96.485	23.061	1	8065.5
cm^{-1}	4.5563x10^{-6}	1.1963x10^{-2}	2.8591x10^{-3}	1.2398x10^{-4}	1

Conversion of polarizability units

1 a.u = 1.649*10^{-41} C^{2}m^{2}J^{-1}

Table 11. *Character table for the C_{2v} point group*

	E	**C_2**	**! $_v$**	**! $_v$'**		
A_1	1	1	1	1	z	x^2, y^2, z^2
A_2	1	1	-1	1	I_z	xy
B_1	1	-1	1	1	x, I_y	xz
B_2	1	-1	-1	1	Y, I_x	yz

! $_v$ is reflection through the zx-plane and ! $_v$' reflection through the zy-plane.

Acknowledgements

I would like to acknowledge Docent Henrik Ottosson for accepting me as a Ph.D student in his research group and providing the opportunity for me to learn more of applied quantum chemistry.

I would also like to thank:

Prof. Raül Crespo and Dr. Carmen Piqueras for the possibility to do a three-month project at Departament de Química Física, Univerisitat de València.

Prof Leif Hammarström for co-supervision, Prof. Sten Lunell for arranging a desk for me at the Department of Quantum Chemistry and Prof. Joshua Smith for collaboration and hospitality in Arcata, California, USA.

Lijlewahls foundation for co-funding the stay in Valencia, Swedish research council (Vetenskapsrådet) for funding, and NSC in Linköping, for supplying invaluable computer resources.

The HO-group, especially; Dr. Ahmed El-Nahas, Dr. Haruhisa Kato and Julius Tibbelin for ideas and discussions regarding the project.

People at the former Department of Organic Chemistry: Dr. Ian Munslow (for corrections of this thesis), Dr. Torben Rasmusen (for discussions and computer related stuff), Dr. Stefan Modin (all technical stuff), Eva Pylvänen (for keeping track of all paperwork) as well as all the other cheerful Ph.D. students, Post Docs and technicians.

People at the Department of Quantum Chemistry, especially; Daniel Norberg, Fil. Lic. Anders Borg.

The good friends; Dr. Magnus Engqvist, Dr. Klas Källström, and Herr Dr. Christian Hedberg. Fredrik Ericsson (also for graphical support).

And most of all Maria, Alfred and the rest of my family.

Summary in Swedish

Simulering av nya potentiella byggstenar för molekylärelektronik

Behovet av molekylärelektronik

I många av de apparater vi dagligen använder finns det någon typ av mikrochip som styr dess funktion. För femtio år sedan hade flertalet av dessa apparater inte varit möjliga att tillverka eftersom elektronikkomponenterna helt enkelt var för stora. De senaste 40 åren har storleken på komponenterna, de minsta byggstenarna, krympt i en accelererande takt. Detta förutspåddes redan i mitten av 1960-talet då Gordon Moore uppskattade att antalet komponenter per mikrochip skulle fördubblas varje år. Tio år senare blev den förutsägelsen känd som ”Moore’s lag” och hade då modifierats till att gälla för cirka 1,5 års perioder. Hur väl denna förminskningsprocess verkligen följer utsagan eller inte ska vara osagt, men att komponentstorleken minskar för varje generation av processorer är ett faktum. Detta faktum kommer att medföra, att vid en tidpunkt inte allt för långt i framtiden (enl. vissa bedömare inom 10-15 år), kommer dagens teknologi mikrochiptillverkning till en fysikalisk gräns varefter ytterligare förminskning blir omöjlig. Om industrin då ska kunna fortsätta förminskningsprocessen kommer det att krävas nya metoder och material. Ett nytt forskningsområde som strävar efter att kunna framställa betydligt mindre komponenter än de nuvarande är molekylärelektronikområdet. Förenklat sett försöker man bygga upp molekyler som kan agera som elektronikkomponenter, istället för som med dagens teknologi försöka etsa ut så små komponenter som möjligt på en platta av kiseloxid.

Kort historik om molekylärelektronik

Idén att använda den molekylära skalan för funktioner som tidigare bara varit påtänkta i den makroskopiska världen är inte ny. Redan år 1959 gav fysikern Richard Feynman en föreläsning där han lade fram idéer att om man kunde göra föremål på molekylär och atomär nivå så skulle svindlande perspektiv öppnar sig. Han gav följande exempel; Om en bokstav kunde motsvaras av en kub på 5*5*5 atomer så skulle den tidens *alla* böcker kunna få plats i ett kubiskt korn med 0,13 mm sidstorlek. I naturen finns också information lagrad på molekylär nivå, t.ex. i det mänskliga DNAt där hela vår

kropps uppbyggnad och utveckling finns lagrad, allt i en makromolekyl som inte ens är synlig för ögat.

Det första förslaget för ett molekylärt system med egenskaper likt en traditionell elektronikkomponent fördes fram 1974 av Ari Aviram och Mark Ratner. Sedan dess har utvecklingen möjliggjort såväl experimentella förutsättningar som teoretiska modeller för att rationalisera hur molekyler ska kunna fungera som elektroniska komponenter. Dock är forskningen och utvecklingen fortfarande i barndomsstadiet där både möjligheterna och svårigheterna är många.

Egenskaper hos molekylära ledare

I denna avhandling är fokus riktat på den enklaste byggstenen inom elektroniken, ledaren. Det har visat sig att de molekyler som bäst leder laddning är så kallade *konjugerade* molekyler. Denna egenskap, konjugation, kan bero på olika egenheter hos den enskilda molekylen men yttrar sig på ungefär samma sätt. Elektronerna i en konjugerad molekyl är mer rörliga, kan delokaliseras lättare, än hos en icke-konjugerad molekyl. Konjugation kan inte mätas på något absolut sätt, utan istället får man undersöka hur konjugationen påverkar andra fysikaliska och kemiska egenskaper.

De egenskaper som här studeras är polariserbarhet, hur en injicerad positiv laddning kan fördelas i en molekyl och hur UV-ljusabsorption ändras mellan vissa molekyler.

Resultat

Datorsimuleringar har använts för att förutsäga egenskaper hos en hittills outforskad klass av molekyler som vi valt att kalla *tunga staffaner* (eng. *heavy-core staffanes* efter engelskans *staff* = stav). Dessa hypotetiska molekyler är likt en kedja uppbyggda av mindre, likadana enheter (monomer) sammanbundna till en stavliknande molekyl, *Figur A*.

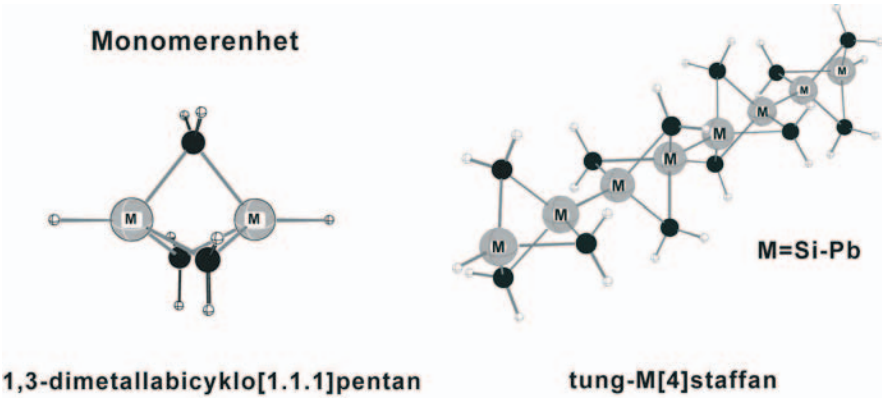

Figur A. Monomerenhet och en tung staffan bestående av fyra monomer enheter. M motsvarar något av atomslagen kisel, germanium, tenn eller bly.

För att få så hög tillförlitlighet som möjligt så har beräkningsmetoder baserade på kvantmekanik använts, d.v.s. man utgår från kvantmekanikens lagar och använder endast ett fåtal approximationer. Detta för att undvika fel som kan uppkomma av de simuleringsmetoder som har optimerats för andra typer av molekyler.

Ringspänning och reaktivitet

Då dessa tunga staffaner ännu inte har tillverkats gjordes en studie i monomer stabilitet och viss mån även deras reaktivitet. Eftersom monomererna består av sammansatta små ringar kommer det att finnas ringspänning i dem. Monomeren där molekylen bara utgörs av kolatomer är sedan tidigare framställd och väl undersökt. Genom att studera molekyler uppbyggda av bara kol med enheter där två atomer i nyckelpositioner har bytts ut mot kisel, germanium, tenn eller bly kan man få en uppfattning om hur ringspänningen påverkas av de olika atomtyperna i dessa två positioner. Det visade sig att ringspänningen för molekyler med kisel, germanium, tenn och bly var lägre med cirka 20 %, vilket är positivt när man ser till möjligheten att kunna framställa dem. Dock gav studien om deras reaktivitet med vatten indikationer på att främst de tenn- och bly-innehållande molekylerna snabbt reagerar med vatten och faller sönder.

Polariserbarhet

Förenklat sett säger polariserbarheten hur lätt och hur mycket elektronerna i en molekyl kan omfördelas om den utsätts för ett elektriskt fält, högre polariserbarhet indikerar på bättre konjugation.

Om man beräknar hur polariserbarheten varierar med längden på kedjan får man en uppfattning om dess konjugation. För en icke-konjugerad molekyl ökar polariserbarheten linjärt med kedjans längd men för en konjugerad molekyl är denna ökning till en början större. Detta ger att polariserbarheten per monomerenhet når ett mättnadsvärde även för konjugerade molekyler.

Resultaten från polariserbarhetsberäkningarna visar att de staffaner med tenn i nyckelpositionerna uppvisar samma storleksordning i avseende på polariserbarhet som välkända konjugerade molekyler som används i experimentella studier av molekylära ledare. Även kisel-innehållande staffaner uppvisar en klart högre polariserbarhet än motsvarande molekyler helt bestående av kol och väte.

Laddningsdelokalisering och reorganisationsenergier

Om en elektron avlägsnas från en molekyl i neutralt tillstånd skapas ett överskott på positiv laddning i molekylen. Besitter molekylen konjugerande förmåga kan laddningen spridas ut, delokaliseras, över den konjugerande delen av molekylen. Om inte detta är möjligt så blir den positiva laddningen lokaliserad till ett mindre antal atomer i molekylen. Detta kan ses om man tittar på hur avstånden mellan de olika atomerna i molekylen förändras med eller

utan laddning. Små förändringar fördelade över hela molekylen indikerar på konjugering medan stora lokala förändringar i avstånd det motsatta.

I fallet med staffaner ser man att de kisel-innehållande staffanerna och, i högre utsträckning, tenn-staffanerna sprider ut laddningen mer än kol-staffanerna.

Om man ser till hur mycket energi det krävs för att atomerna i en staffanmolekyl ska flytta på sig för att kunna anpassa sig till den nya laddningen, så får man ett mått på en av de faktorer som avgör hur bra ledningsförmåga bulkmaterial bestående av staffaner har.

Återigen visar sig samma trend som tidigare, mindre energi krävs for tenn-staffanen jämfört med kisel-staffanen, som i sin tur behöver mindre energi än kol-staffanen.

Ljusabsorption

En konjugerad molekyl absorberar ljus med lägre energi ju längre den blir eller om konjugationen ökar. För att undersöka hur storleken på monomerenheten påverkar dess ljusabsorbtion utfördes beräkningar på två olika grund molekyler med olika långa kolbryggor mellan två kisel-kisel bindningar.

Beräkningarna förutspår att ju mindre burstruktur som sammanlänkar de två kisel-kisel bindningarna destå mindre energi behövs för att molekylen ska börja absorbera ljus. Detta ger stöd för hypotesen om att ett kortare avstånd inom burstrukturen och kortare kolbryggor påverkar konjugationen positivt.

Slutsats

Denna studie har visat att:

- Monomererna i kisel-, germanium-, tenn- och bly-staffaner förutsägs var mindre ringspända än motsvarande existerande kol-staffaner. Detta utan att deras reaktivitet med vatten förväntas vara hög, undantaget tenn- och bly-monomererna.
- Beräkningar av polariserbarheter, laddningsdelokalisering och reorganisationsenergi visar att kisel- och framförallt tenn-staffaner uppvisar konjugationseffekt i klass med vissa idag använda molekylära ledare.
- Burstrukturens storlek och kolbryggornas längd har betydelse för konjugationen i dessa typer av molekyler.

Avslutningsvis bedöms dessa molekyler vara så pass intressanta molekylära ledare att arbete för att realisera dem pågår för att möjliggöra ytterligare några byggstenar inom molekylär elektronik.

References

[1] http://nobelprize.org/
[2] G. E. Moore *Electronics Magazine* **1965**, *38*.
[3] Talk given on December 29th 1959 at the annual meeting of the American Physical Society at the California Institute of Technology (Caltech).
[4] A. Aviram, M. A. Ratner *Chem. Phys. Lett.* **1974**, *29*, 277.
[5] M. A. Reed, C. Zhou, C. J. Muller, T. P. Burgin, J. M. Tour *Science* **1997**, *278*, 252.
[6] C. P. Collier, G. Mattersteig, E. W. Wong, Y. Luo, K. Beverly, J. Sampaio, F. M. Raymo, J. F. Stoddart, J. R. Heath *Science* **2000**, *289*, 1172.
[7] R. F. Service *Science* **2001**, *294*, 2442.
[8] "Schön papers pulled" *Science* **2002**, *298*, 513.
[9] R. F. Service *Science* **2003**, *302*, 556.
[10] X.-M. Yan, A. M. Contreras, M. M. Koebel, J. A. Liddle, G. A. Somorjai *Nano lett.* **2005**, *5*, 1129.
[11] P. M. Ajayan, *Chem. Rev.* **1999**, *99*, 1787.
[12] L. A. Bumm, J. J. Arnold, M. T. Cygan, T. D. Dunbar, T. P. Burgin, L. Jones II, D. L. Allara, J. M. Tour, P. S. Weiss *Science* **1996**, *271*, 1705.
[13] A. Tsuda, A. Osuka *Science* **2001**, *293*, 79.
[14] N. W. Ashcroft, N. D. Mermin *Solid State Physics Int. Ed.* **1974**.
[15] M. Bruschi, M. G. Giuffreda, h. P. Luthi *Chimia* **2005**, *59*, 539.
[16] H. S. Plitt, J. W. Downing, M. K. Raymond, V. Balaji, J. Michl *J. Chem. Soc. Faraday Trans.* **1994**, *90*, 1653.
[17] R. D. Miller, J. Michl *Chem. Rev.* **1989**, *89*, 1359.
[18] P.W. Anderson *Phys. Rev.* **1958**, *109*, 1492.
[19] M. C. Piqueras, R. Crespo, J. Michl *J. Chem. Phys.* **2003**, *107*, 4661.
[20] P. F. H. Schwab, M. D. Levin, J. Michl *Chem. Rev.* **1999**, *99*, 1863
[21] E. W. Della, C. A. Grob, D. K. Taylor *J. Am. Chem. Soc.* **1994**, *116*, 6159.
[22] A. J. McKinley, P. N. Ibrahim, V. Balaji, J. Michl *J. Am. Chem. Soc.* **1992**, *114*, 10631.
[23] W. Heitler, F. London *Z. Physik*, **1927**, *44*, 455.
[24] G. G. Hall *Proc. R. Soc.* (London), **1951**, A205, 541.
[25] P-O Löwdin *Phys. Rev.*, **1954**, *97*, 1447.
[26] C. Lee, W. Yang, R. G. Parr *Phys. Rev. B.* **1988**, *37*, 785.
[27] A. D. Becke *J. Chem. Phys.* **1993***, 98*, 1372.
[28] P. J. Stephens, F. J. Devlin, C. F. Chabalowski, M. J. Frisch *J. Phys. Chem.* **1994**, *98*, 11623.
[29] M. A.Spackman *J. Phys. Chem.* **1989**, *93*, 7594, and references there in.
[30] A. J. Sadlej *Collect. Czech. Chem. Commun.* **1998**, *53*, 1995.
[31] P. J. Hay, W. R. Wadt *J. Chem. Phys.* **1985**, *82*, 270; P. J. Hay, W. R. Wadt *J. Chem. Phys.* **1985**, *82*, 284; P. J. Hay, W. R. Wadt *J. Chem. Phys.* **1985**, *82*, 299.

[32] J. M. L. Martin, A. Sundermann *J. Chem. Phys.* **2001**, *114*, 3408.
[33] T.O. Faust, J.M. Bailey, B.J. Wright, T.M. Gilbert, L.S. Sunderlin, *J. Phys. Chem. A* **2001**, *105*, 8111.
[34] W. J. Hehre, R. Ditchfield, L. Radom, J. A. Pople *J. Am. Chem. Soc.* **1970**, *92*, 4796.
[35] P. George, M. Trachtman, C. W. Bock, A. M. Brett *Tetrahedron* **1976**, *32*, 317.
[36] K. B. Wiberg. F. H. Walker *J. Am. Chem. Soc.* **1982**, *104*, 5239.
[37] K. B. Wiberg, D. S. Connor, G. M. Lampman *Tetrahedron Lett.* **1964**, 531.
[38] P. E. Eaton, G. H. Temme *J. Am. Chem. Soc.* **1973**, *95*, 7508.
[39] F. W. Semmler, K. Bartelt *Ber. Dtsch. Chem. Ges.* **1907**, *40*, 4844.
[40] N. Takaishi, Y. Inamoto, K. Tsuchihashi, K. Yashima, K. Aigami *J. Org. Chem.* **1975**, *40*, 2929.
[41] M. Doyle, W. Parker *Tetrahedron Lett.* **1970**, *42*, 3619; b) N. J. Leonard, J. C. Coll *J. Chem. Soc.* **1970**, *92*, 6685.
[42] a) Y. Zhang, J. Smith, D. M. Lemal *J. Am. Chem. Soc.* **1996**, *118*, 9454. b) Y. He, C. P. Junk, J. J. Cawley, D. M. Lemal *J. Am. Chem. Soc.* **2003**, *125*, 5590.
[43] Y. Kabe, T. Kawase, J. Okada, O. Yamashita, M. Goto, S. Masamune *Angew. Chem. Int. Ed. Engl.* **1990**, *29*, 794.
[44] a) L. R. Sita, R. D. Bickerstaff *J. Am. Chem. Soc.* **1989**, *111*, 6454; b) L. R. Sita, I. Kinoshita *J. Am. Chem. Soc.* **1990**, *112*, 8839.
[45] L. R. Sita, I. Kinoshita *J. Am. Chem. Soc.* **1991**, *113*, 5070.
[46] a) N. Choi, K. Asano, W. Ando *Organometallics* **1995**, *14*, 3146; b) H. Yoshida, Y. Takahara, T. Erata, W. Ando *J. Am. Chem. Soc.* **1992**, *114*, 1098.
[47] T. Iwamoto, D. Yin, C. Kabuto, M. Kira *J. Am. Chem. Soc.* **2001**, *123*, 12730.
[48] K. B. Wiberg, F. H. Walker *J. Am. Chem. Soc.* **1982**, *104*, 5239.
[49] U. Herzog, G. Rheinwald *Eur. J. Inorg. Chem.* **2001**, 3107.
[50] a) K. Tamao, M. Kumada, A. Noro *J. Organomet. Chem.* **1971**, *31*, 169. b) D. Casher, H. Tsuji, A. Sano, M. Katkevics, A. Toshimitsu, K. Tamao, M. Kubota, T. Kobayashi, C. H. Ottosson, D. David, and J. Michl *J. Phys. Chem. A* **2003**, *107* , 3559.
[51] K. B. Wiberg *J. Am. Chem. Soc.* **1983**, *105*, 1227.
[52] D. Kitchen, J. Jackson, L. Allen *J. Am. Chem. Soc.* **1990**, *112*, 3408.
[53] M. D. Levin, P. Kaszynski, J. Michl *Chem. Rev.* **2000**, *100*, 169.
[54] O. Jarosch, R. Walsh, G. Szeimies *J. Am. Chem. Soc.* **2000**, *122*, 8490.
[55] W. Adcock, M. J. Brunger, C. I. Clark, I. E. McCarthy, M. T. Michalewicz, W. von Niessen, W. Weigold, D. A. Winkler *J. Am. Chem. Soc.* **1997**, *119*, 2896.
[56] M. Takahashi, K. Hatano, Y. Kawada, G. Koga, N. Tokitoh, R. Okazaki *J. Chem. Soc., Chem. Commun*. **1993**, 1850.
[57] a) N. Rot, T. Nijbacker, R. Kroon, F. J. J. de Kanter, F. Bickelhaupt, M. Lutz, A. L. Spek *Organometallics* **2000**, *19*, 1319; b) M. A. Dam, F. J. J. Kanter, F. Bickelhaupt, W. J. J. Smeets, A. L. Spek, J. Fornies-Camer, C. Cardin *J. Organomet. Chem.* **1998**, *550*, 347; c) M. A. Dam; M. W. J. Hoogervorst, F. J. J. de Kanter, F. Bickelhaupt, A. L. Spek *Organometallics* **1998**, *17*, 1762; d) M. A. Dam; O. S. Akkerman, F. J. J. de Kanter, F. Bickelhaupt, N. Veldman, A. L. Spek *Chem. Eur. J.* **1996**, *9*, 1139.
[58] A. Bondi, *J. Phys. Chem.* **1964**, *68*, 441. Only van der Waals radii from Pauling's approximation (r_b) and based on half the de Broglie wave lengths ($_B/2$) are available for C, Si, Ge, and Sn. The values in Å are as follows: C (r_b = 1.53, $_B/2$ = 1.82), Si (r_b = 1.93, $_B/2$ = 2.15), Ge (r_b = 1.98, $_B/2$ = 2.19), Sn (r_b = 2.16, $_B/2$ = 2.27).

[59] W. Parker, W. V. Steel, I. Watt *J. Chem. Thermodynamics* **1977**, *9*, 307.
[60] H. Schumann, H. Benda *Angew. Chem.* **1969**, *24*, 1049.
[61] F. Garcia, A. D. Hopkins, S. M. Humphrey, M. McPartlin, C. M. Pask, , A. D. Woods, D. S. Wright *Organometallics* **2004**, *23*, 4821.
[62] J. Gerratt, I. M. Mills *J. Chem. Phys.* **1968**, *49*, 1719.
[63] G. Weck, A.Milet, R. Moszynski, E. Kochanskia *J. Mol. Struct. (Theochem)* **2002**, *591*, 141.
[64] K. G. Denbigh *Trans. Faraday Soc.* **1940**, *36*, 936.
[65] P. L. Davies *Trans. Faraday Soc.* **1952**, *48*, 789.
[66] T. K. Ghanty, S. K. Ghosh *J. Chem. Phys.* **2003**, *118*, 8547.
[67] E. K. Dalskov, J. Oddershede, D. M. Bishop *J. Chem. Phys.* **1998**, *108*, 2152.
[68] R. Stowasser, R. Hoffman *J. Am. Chem. Soc.* **1999**, *121*, 3414.
[69] C. Adamo, M. Cossi, G. Scalmani, V. Barone, *Chem. Phys. Lett.* **1999**, 265.
[70] P. Otto, A. Martinez, A. Czaja, J. Ladik, *J. Phys. Chem.* **2002**, *117*, 1908.
[71] B. Kirtman, M. J. Hasan *J. Chem. Phys.* **1992**, *96*, 470.
[72] G. J. B. Hurst, M. Dupuis, E. Clementi *J. Chem. Phys.* **1988**, *89*, 385.
[73] J. Michl, R. West *Acc. Chem. Res.* **2000**, *33*, 821.
[74] J.-M. André, J. Delhalle, J. L. Brédas In *Quantum Chemistry Aided Design of Organic Polymers: An Introduction to the Quantum Chemistry of Polymers and its Applications*, World Scientific Publishing Ltd, **1991**, Singapore, pp. 312.
[75] a) J. M. Tour *Chem. Rev.* **1996**, *96*, 537. b) J. L. Brédas, D. Beljonne, V. Coropceanu, J. Cornil *Chem. Rev.* **2004**, *104*, 4971. c) P. F. H. Schwab, J. R. Smith, J. Michl *Chem. Rev.* **2005**, *105*, 1197.
[76] B. Q. Xu, X. L. Li, X. Y. Xiao, H. Sakaguchi, N. J. Tao *Nano Lett.* **2005**, *5*, 1491.
[77] B. Jansik, B. Schimmelpfennig, P. Norman, Y. Mochizuki, Y. Luo, H. J. Ågren *J. Phys. Chem. A* **2002**, *106*, 395.
[78] I. Ciofini, C. Adamo, H. Chermette *J. Chem. Phys.* **2005**, *123*, 121102.
[79] D. Jacquemin, E. A. Perpète. I. Ciofini. C. Adamo *Chem. Phys. Lett.* **2005**, *405*, 376.
[80] (a) M. Kobayashi, J. Chen, T.-C. Chung, F. Moraes, A. J. Heeger, F. Wudl, *Synth. Met.* **1984**, *9*, 77. (b) T.-C. Chung, J. Kaufman, A. J. Heeger, F. Wudl, *Phys. Rev. B* **1984**, *30*, 702.
[81] (a) K. Yakushi, L. J. Lauchlan, T. C. Clarke, G. B. Street, *J. Chem. Phys.* **1983**, *79*, 4774. (b) J. B. Brédas, J. C. Scott, K. Yakushi, G. B. Street, *Phys. Rev. B.* **1984**, *30*, 1023.
[82] J. V. Ortiz *J. Chem. Phys.* **1988**, *89*, s6348.
[83] G. R. Hutchison, M. A. Ratner, T. J. Marks, *J. Am. Chem. Soc.* **2005**, *127*, 2339.
[84] J. E. Carpenter, F. Weinhold, *J. Mol. Struct. (Theochem)* **1988**, *41*, 169.
[85] V. M. Geskin, A, Dkhissi, J. L. Bredas, *Int. J. Quant. Chem.* **2003**, *91*, 350.
[86] F. A. Cotton, *Chemical Applications of Group Theory*, 2nd ed. Wiley **1971**.
[87] P. A. Malmqvist, B. O. Roos, *Chem. Phys. Lett.* **1989**, *155*, 189.
[88] J. Finley, P. A. Malmqvist, B. O. Roos, L. Serrano-Andre´s, *Chem. Phys. Lett.* **1998**, 288, 299.
[89] N. Forsberg, P. A. Malmqvist, *Chem. Phys. Lett.* **1997**, *274*, 196.
[90] Miller, R. D.; Michl, J. *Chem. Rev.* **1989**, *89*, 1359.
[91] D. L. Casher, H. Tsuji, A. Sano, M. Katkevics, A. Toshimitsu, K. Tamao, M. Kubota, T. Kobayashi, H. C. Ottosson, D. E. David, J. Michl, *J. Phys. Chem. A* **2003**, *107*, 3559.

[92] N. Wiberg, H. Schuster, A. Simon, K. Peters, Angew. Chem. Int. Ed. **1986**, *25*, 79. N. Wiberg, W. Niedermayer,H. Noth, J. Knizek, W. Ponikwar, K. Polborn *Naturforsch*, **2000**, 55b, 389.

Acta Universitatis Upsaliensis

Digital Comprehensive Summaries of Uppsala Dissertations from the Faculty of Science and Technology 271

Editor: The Dean of the Faculty of Science and Technology

A doctoral dissertation from the Faculty of Science and Technology, Uppsala University, is usually a summary of a number of papers. A few copies of the complete dissertation are kept at major Swedish research libraries, while the summary alone is distributed internationally through the series Digital Comprehensive Summaries of Uppsala Dissertations from the Faculty of Science and Technology. (Prior to January, 2005, the series was published under the title "Comprehensive Summaries of Uppsala Dissertations from the Faculty of Science and Technology".)

Distribution: publications.uu.se
urn:nbn:se:uu:diva-7492

ACTA
UNIVERSITATIS
UPSALIENSIS
UPPSALA
2007